
OBSERVATIONS OF SALT CRUST THICKNESS CHANGE AT THE BONNEVILLE SALT FLATS FROM 2003-2016

Brenda B. Bowen^{1,2*}, Evan L. Kipnis¹, and Jessie M. Pechmann³

ABSTRACT

The salt-paved landscape of the Bonneville Salt Flats (BSF) in northwestern Utah is a unique resource for the state. It is a historic landmark for land speed racing and has been a source of economic mineral resources for over a century. It is also a landscape that changes actively in response to geologic fluctuations in hydrology and composition unrelated to human uses. Perceptions of changes in the salt crust at BSF have led to quasi-decadal analysis of the volume of saline strata present in this area since the mid-century. In fall 2016, the most recent iteration of the BSF salt crust thickness study was conducted, and 69 shallow sediment cores were collected from BSF to measure the total volume of salt crust present in this environment at this time. The cores were collected in the same location as the previous study conducted in 2003. The salt crust package of sediments at BSF includes interbedded and laterally discontinuous layers of crystalline halite (NaCl) and gypsum ($\text{CaSO}_4 \cdot 2\text{H}_2\text{O}$) sand. Total salt crust thickness values range from < 0.5 cm around the perimeter, to ~ 1.5 m in the center with a generally lens-shaped geometry. The total salt crust measured in September 2016 was composed of 35% halite and 65% gypsum sand and included a total volume of 67,464,024 m^3 . This suggests an overall $\sim 7\%$ volume decrease in the total salt crust since 2003, and a 17% decrease in the relative amount of observed halite versus gypsum. Different approaches in 2003 and 2016 for measuring and calculating total salt crust volume add complexity to interpretations of change over time, particularly with respect to the internal composition of the salt crust stratigraphy. Spatial analysis of changes in the salt crust shows that most of the observed salt crust thinning and reduction in total halite thickness has occurred along the northwest perimeter of the salt crust, coincident with the topographic low and the general location of the historic Bonneville Speedway. Ongoing research aims to link the observed changes in the salt crust with processes that are impacting the landscape over human to geologic time scales.

INTRODUCTION

The Bonneville Salt Flats (BSF) are a perennial salt pan that covers an area over ~ 75 km^2 in westernmost Utah, and like the Great Salt Lake, is a remnant of Pleistocene Lake Bonneville (figure 1; Oviatt, 2015). The West Desert includes multiple basin and range playa systems, but BSF is the only one that presently has a persistent surface halite salt crust that is seasonally repaved through cycles of flooding, evaporation, and desiccation (Bowen and others, 2017). As with all salt pan systems, the landscape of BSF is temporally dynamic and changes throughout the year in response to changes in hydrology, water balance, salt growth, and dissolution (Lowenstein and Hardie, 1985). The perennial halite surface at BSF has led to a unique history of land use with the extensive use of the landscape for automobile racing (Noeth, 2002). In addition, potash mining has occurred from extraction of groundwater brines associated with the salt

crust for a century (Nolan, 1928). Past research has demonstrated that potash mining has impacted the composition and hydrology of the salt crust system (Mason and Kipp, 1998) and for the last twenty years, an experimental “Salt Laydown” project has aimed to mitigate the impacts of long-term extraction (White, 2004). Effective and sustainable management of this valued landscape requires a quantitative understanding of how the system is changing over time and the role of extraction and land use in modifying the landscape.

The objective of this work was to 1) measure the thickness and volume of the BSF salt crust and 2) compare these data to similar measurements of BSF made in 2003 by White and Terrazas (2006) to evaluate how the salt crust has changed through time. Similar studies have been conducted every ~ 13 years since 1960, and results have ranged from interpretations of extreme decrease in volume in the 1970s and 1980s to essentially no observed

¹Geology and Geophysics, University of Utah, Salt Lake City, UT, USA, brenda.bowen@utah.edu,

²Global Change and Sustainability Center, University of Utah, Salt Lake City, UT, USA

³Professional Masters of Science and Technology, University of Utah, Salt Lake City, UT, USA

Bowen, B.B., Kipnis, E.L., and Pechmann, J.M., 2018, Observations of salt crust thickness change at the Bonneville Salt Flats from 2003-2016, *in* Emerman, S.H., Bowen, B., Schamel, S., and Simmons, S., editors, *Geofluids of Utah: Utah Geological Association Publication 47*, p. 247–285.

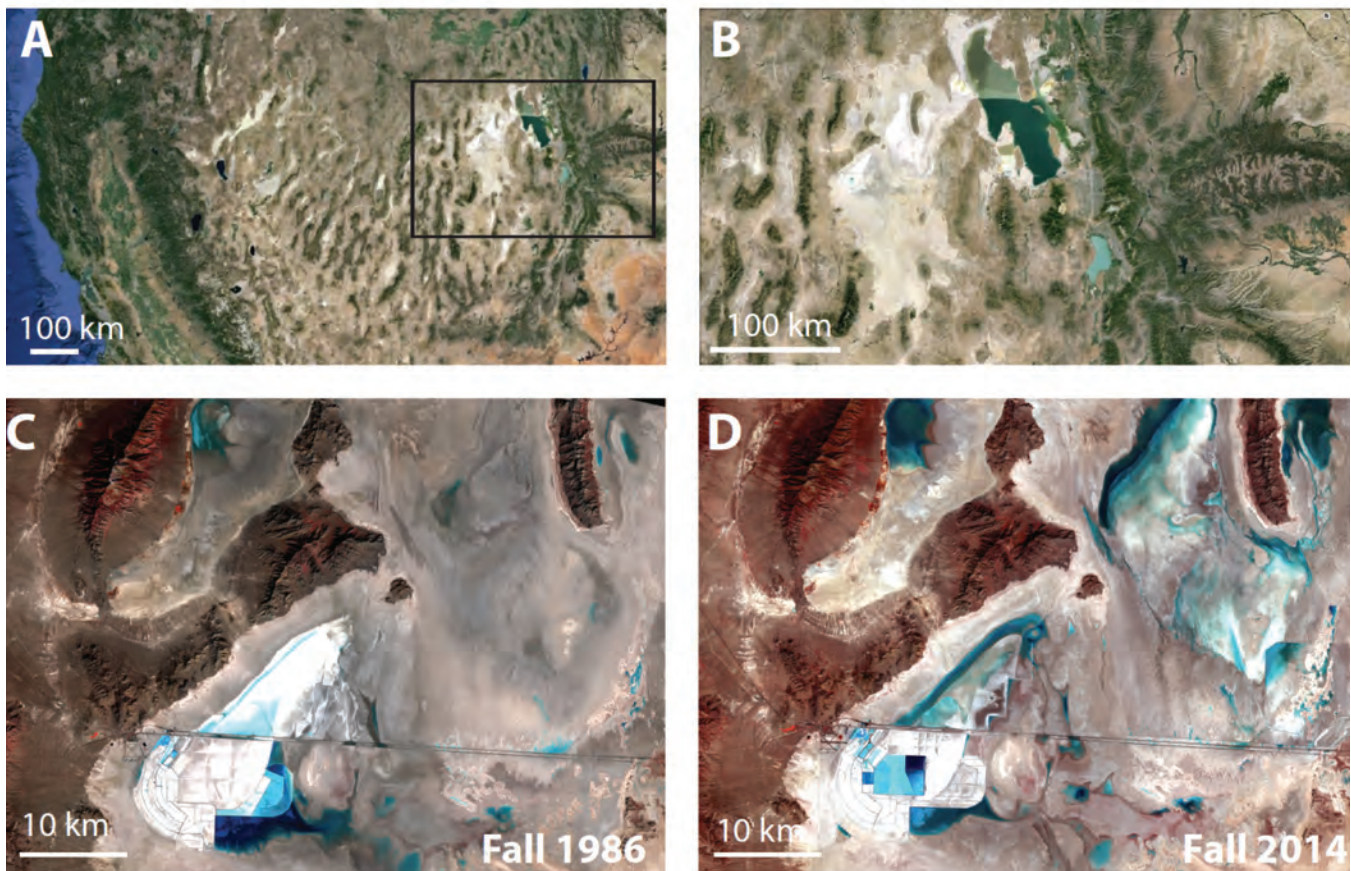


Figure 1. Location of the Bonneville Salt Flats. A) Regional context within the western U.S. B) BSF occupies the westernmost edge of the Great Salt Lake Desert. C and D) False color Landsat satellite data showing an example of differences in the landscape over decadal time scales, including footprint of surface water (blue), in fall 1986 and fall 2014.

change from 1988 to 2003 (McMillan, 1974; Brooks, 1991; White and Terrazas, 2006). The Bureau of Land Management (BLM) approved the Intrepid Potash Mine and Reclamation Plan in 2012 with the requirement of a 2018 Salt Study: “The operator/lessee shall arrange for a third party contractor with oversight from BLM to repeat the BLM’s 2003 salt-crust thickness study on the BSF by the end of 2018.” (EA #UT-020-2006-002, 2012). The work presented here fulfills that requirement and provides new insights into the current state of the BSF salt crust, analysis of the stratigraphy, and a detailed evaluation of how the morphology of the salt crust has changed since 2003.

METHODS

Core Drilling

The locations of the sites analyzed in the 2003 salt crust thickness study (White and Terrazas, 2006) were identified using records of latitude and longitude coordinates and hand-held GPS units. From September 5 – 8, 2016, 69 cores directly adjacent to the sites described in the 2003 study were drilled or augered, described, and sampled. At several of the sites, wooden stakes placed in

2003 were still present. Major Drilling America, Inc. was contracted to help to core the entire “salt crust” (gypsum and halite package) at each of the sites. Forty-five of the sites were cored using a track mounted mini sonic rig (figure 2). Sonic drilling does not require the use of drilling fluids, which is important in a soluble evaporite setting such as BSF. In addition, the sonic vibrations ideally prevent the need for rotational sampling, which is preferable for obtaining undistorted sediment cores in unlithified and fluid-saturated systems such as BSF. Four-inch diameter cores were sampled in a core barrel, carefully transferred to a plastic bag (figure 2E), and collected into three-foot long core boxes (figure 2F). Coring depths ranged from ~0.6 m (~2 ft) to > 2 m (~7 ft) depending on the amount of evaporite strata present in the subsurface at a particular site. At each site, core sampling aimed to extend at least ~0.5 m (~1-2 ft) past the base of the salt crust strata into the underlying fine-grained laminated mud sediments that do not contain bedded evaporites. The sonic rig was mounted onto the back of an 18-wheel tractor-trailer with a custom hole cut through the trailer bed to allow the sonic rig access to the salt crust without demobilizing the drill rig (which would have had a larger impact on the salt crust and would have taken significantly more time).

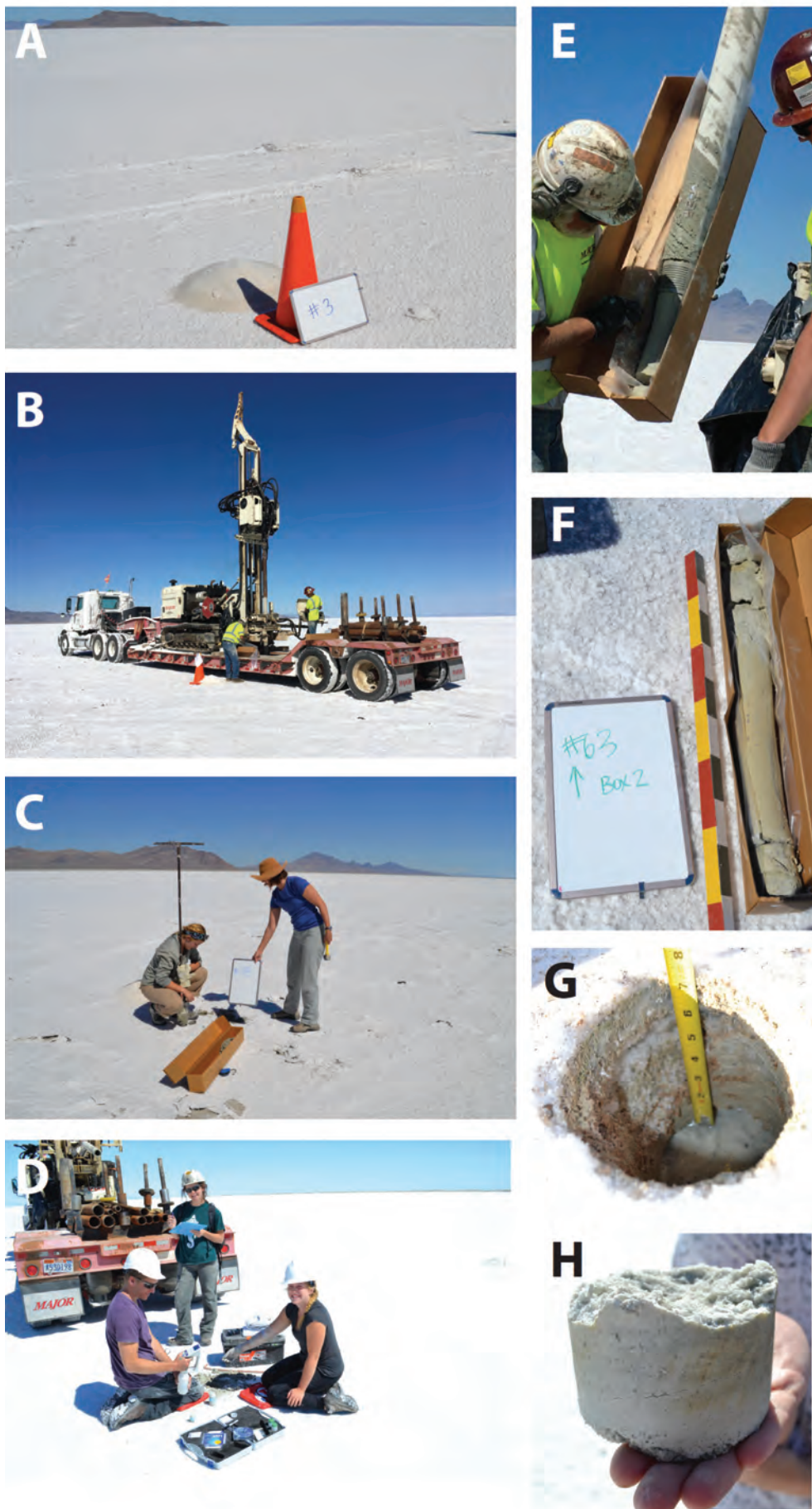


Figure 2. Photographs of field operations during coring in September of 2016. A) Drill sites were located and staged with ~8 gallons of granular halite salt (provided by Intrepid Potash) to back-fill drill holes. B) Major Drilling sonic rig on a tractor trailer. C) Hand auger used where necessary (where access with sonic rig was not possible due to sensitivity of surface). D) Field team analyzing groundwater after coring. E) Sediment being fed from core barrel into core box. F) Field-based descriptions were made for each core. G) Down-hole measurements of strata were made as possible. H) An example of somewhat-lithified halite-cemented fine grained gypsum sand that remained intact.

At the time of sampling, the unlithified saline sediment cores were saturated with shallow saline groundwater, which increased the difficulty of retrieving intact and continuous cores. In addition, the extreme hardness and brittle texture of the uppermost surface halite crust at some sites limited the ability to core through the sediments with one single push of the sonic rig, also making continuous sampling of the sediment difficult. As a result, two cores (D-31 and D-21) out of the 69 sites had poor recovery (38% and 51%), 10 cores had 73%-93% recovery, and the remaining 57 cores (83% of those sampled) had near complete (> 98%) recovery (appendix A). The underlying laminated carbonate mud sediments were highly amenable to sonic coring and sampling with excellent recovery (came out of the core barrel like toothpaste). This was used to increase confidence in the total measured salt crust thickness by noting the total depth that the drillers pushed to in the field (e.g., 2.1 m or 7 ft), and the amount of fine-grained pre-salt sediment that was sampled (e.g., 0.6 m or 2 ft), allowing for calculation of the total salt crust package (e.g., 2.1 m – 0.6 m = 1.5 m or 7 ft – 2 ft = 5 ft). Immediately after extraction, cores were measured and the composition (crystalline halite versus gypsum sand, etc.) was described in the field (e.g., figure 3). Thicknesses of all unique stratigraphic layers were measured, and textures were examined using visual inspection and a hand lens (e.g., halite is much more soluble than gypsum, so a small spray bottle of water was used to spray grains to determine relative solubility). After the cores were extracted, the in-hole stratigraphy was texturally described to note the depths and thicknesses of the stratigraphic intervals from the surface downward as far as possible (~1 m or ~3 ft with an arm). Finally, the depth of the distinctive textural transition at the stratigraphic contact between the salt crust strata and the underlying fine grained sediments was measured using a ~3 m metal pole with a 90 degree bend at the end (similar to the UDOT pole used in the 2003 study). At sites where groundwater filled the drill holes (n = 46), the depth to water was measured.

At 24 of the sites around the perimeter of the salt crust, the drill rig was not appropriate for sampling (not necessary due to lack of surface halite and shallow depths of gypsum sand, and limited vehicular access on the sensitive salt crust), and thus these sites were sampled using a hand auger (figures 2C and 4). At these sites, the uppermost halite crust was < 2 cm thick and was underlain by < 60 cm of massive to laminated gypsum sand above the fine-grained laminated mud sediments. The auger sites typically did not reach groundwater.

All holes at the core sites were backfilled with granular halite provided by Intrepid Potash (figure 2A) and the location of drill sites was identified on the surface using

photoreactive (disappearing) dye provided by the racing community that disappeared within a couple of weeks. The perimeter of the surface halite layer was mapped using visual inspection and a differential GPS unit (figure 4), although the 2016 field-mapped perimeter data were ultimately not used in the analyses of the current salt crust volume (see Results). Surface elevation was measured to ± 10 cm at each core site using a differential GPS unit (figure 5).

Core Analysis

The core samples were transported to the Department of Geology and Geophysics at the University of Utah in Salt Lake City, Utah, and stored in ambient building conditions in laboratory space maintained by B.B. Bowen. Over the three months following coring, all samples were re-examined in detail and all sedimentary strata were re-measured and described based on macroscopic textures (appendix B). Laboratory stratigraphic data were compiled with field observations to develop the most accurate stratigraphic record possible. Representative samples of each unique stratigraphic unit in each core were subsampled, lightly rinsed to remove surface contamination from coring (gently washing clays off surface), and gently pulverized by hand using a mortar and pestle.

The relative concentrations of Cl (chloride) and S (sulfur) were quantified using a Bruker Tracer3 pXRF on a representative samples of all strata from 12 cores (D-2, D-8, D-12, D-24, D-33, D-34, D-35, D-42, D-45, D-55, D-60, and D-66; figure 8A; all cores shown in figure 7) and analyzed for 90 seconds using a blue (Ti) filter under a helium vacuum and reported as total photon counts (appendix D).

The total salt crust thickness is defined as the distance from the ground surface to the bottom of the saline minerals (gypsum and halite) and/or the top of the underlying fine-grained unit (the salt-clay boundary; figure 6). All stratigraphic designations and thicknesses of strata are listed in appendix B. Sediment classification initially followed the organization used by White and Terazzas (2006) and includes dense crystalline halite (DCH), coarse porous halite (CPH), loose aggregated halite (LAH), gypsum sand (GYP), clay, and laminated mud (LAM). Labels for specific sediment types are numbered based on the sequential occurrence of those sediment types down hole and do not indicate lateral correlation. For example, GYP 4 from one core does not necessarily correlate with GYP 4 from another core. Rather, these are both the 4th layer in each core and composed of gypsum. It was determined that the textural classification used for halite in 2003 (e.g., DCH, CPH, LAH) was not distinguishable in many of the 2016 samples, so all halite was grouped as a single sediment type. It was also noted that different gypsum beds had significantly different grain

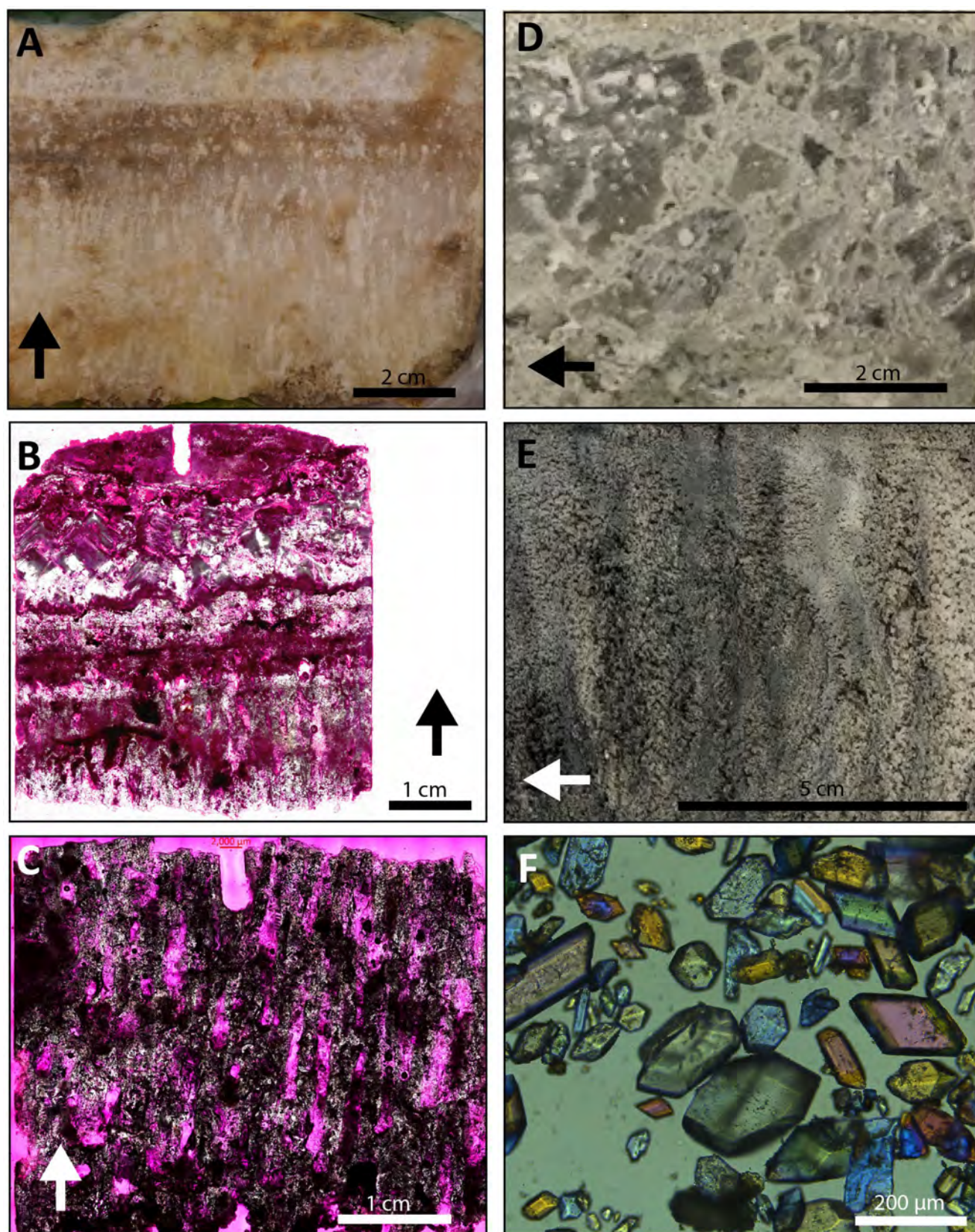


Figure 3. Examples of halite (A, B, C, D) and gypsum (E, F) beds from BSF; arrows indicate up direction. A) Bedded crystalline halite from the uppermost salt crust (near D-54). B) halite crust sample prepared for microscopic analysis (pink epoxy shows pore space). C) example of vertical dissolution pipes within halite crust (pink epoxy shows pore space). D) subsurface halite with a very different halite crystal texture (compared to surface bedded halite) indicative of subsurface formation of salt crystals (D-42). E) fine grained gypsum sand layers with dark grey biofilm (D-35). F) microscopic polarized view of euhedral gypsum grains.

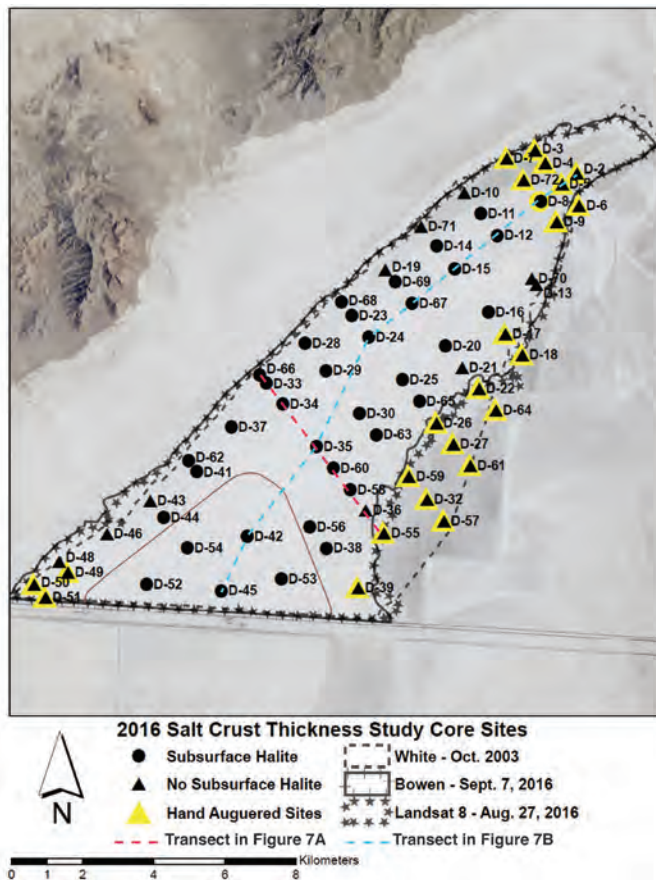


Figure 4. Location of 2003 boreholes and 2016 cores; those hand-augered in 2016 ($n = 24$); those sites with no subsurface halite; location of Salduro Loop berm (brown line); perimeter of halite surface mapped in 2003 and 2016; boundary calculated from Landsat 8 data (after Bowen and others, 2017). The boundary mapped by White in 2003 was used in this study. Red dashed line trending NW to SE shows location of cross section shown in figure 7A. Blue dashed line trending SW to NE shows location of cross section shown in figure 7B.

size characteristics, so these were broken out into separate textural groups in stratigraphic descriptions (e.g., fine grained gypsum, coarse grained gypsum; e.g., figure 10B), but grouped as gypsum sediment for overall analyses (figure 7). The 2016 core data were entered into an Excel spreadsheet along with data from 2003 (White and Terrazas, 2006; appendices) for comparisons between overall measurements and sediment types observed at each site (figure 8).

Geospatial Analysis

ESRI's GIS (Geographic Information Systems) Suite Software was used to study and replicate the methods of the BSF salt crust thickness study conducted by the BLM in 2003 (White and Terrazas, 2006; details about GIS methods in [appendix E](#)). Field point observation maps for 2003 and 2016 were created to identify initial spatial patterns and validate recorded salt thickness data for

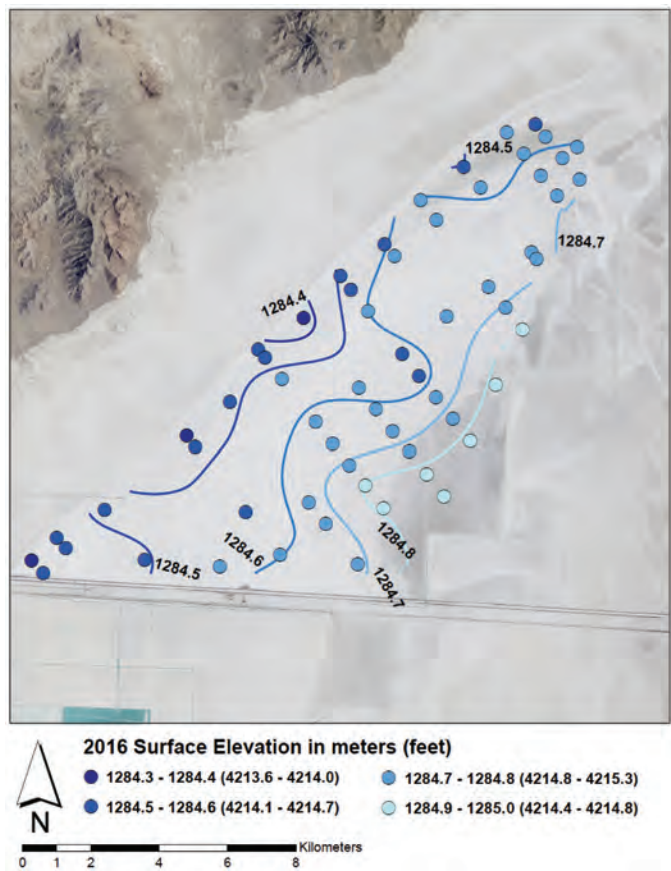


Figure 5. Core locations (dots) and ground surface elevation as measured in September 2016 using a field-based differential GPS with ± 10 cm vertical resolution. The surface is ~ 55 cm (~ 1.8 ft) lower along the northwest edge, sloping upward towards the berms bounding the salt crust on the east.

each field site (figures 6 and 9). ArcGIS Geostatistical Analyst's Geostatistical Wizard was used to interpolate between core sites using ordinary kriging. Kriging assumes that at least some of the spatial variation observed in natural phenomena can be modeled by random processes with spatial autocorrelation, and requires that the spatial autocorrelation be explicitly modeled (Oliver and Webster, 1990). To create maps that display the spatial differences in composition at BSF between 2003 and 2016, a simple difference between interpolated values from the kriging results was calculated. This method was utilized to map the difference from the multiple kriging results for measurements of total salt crust thickness, thickness of the top layer of dense crystallized halite, and total salt thickness of halite and gypsum per each borehole. Continuous thickness surfaces were mapped across the BSF for 2003 and 2016 to show spatial patterns in salt thickness, thickness of the top layer of dense crystallized halite, the total salt thickness of halite and gypsum per each borehole, and to calculate the total salt crust volume.

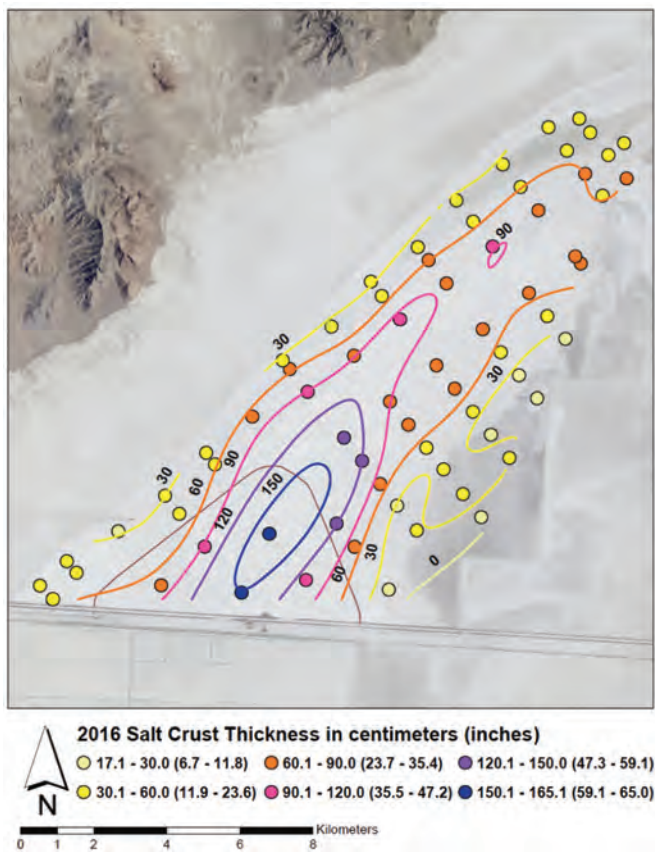


Figure 6. 2016 total salt crust thickness measurements (point data in cm) and 30 cm (~1 ft) isopachs. The “salt crust” is defined as all strata containing evaporite sediments (halite + gypsum) above the underlying fine grained and clay-rich carbonate sediments. Location of Salduro Loop berm shown in brown.

RESULTS AND DISCUSSION

Salt Crust Surface Area

In order to calculate a volume, a 2D surface area must be selected to define the boundaries of BSF. In past studies, the area included in the study varied through time, depending on the spatial extent of surface halite during that particular season or on the location of specific thickness contours. Changing the area greatly impacts the calculated total volume of saline strata, even if the thickness of the salt crust has not changed significantly. Surface area of halite coverage at BSF changes significantly as a function of ponded surface water, temperature, amount of halite dissolution, wind speeds and directions, and evaporation through time (Bowen and others, 2017). The area of surface halite was mapped in the field at the time of coring, as well as using satellite remote sensing methods (figure 4). However, these results are not appropriate for use in calculating overall salt crust volume since, in many areas around the perimeter of the salt crust, the uppermost halite crust was only ~1.5 mm (1/16 in) thick and is not directly connected to the overall subsurface lens of interbedded halite and

gypsum that creates the landscape of BSF. In fact, no subsurface halite was observed at 33 of the sites along the SW, NE, and E boundaries of BSF.

One of the first steps in the GIS analysis was to recreate results of the 2003 salt crust thickness study using the 2003 data (White and Terrazas, 2006). While overall patterns are similar, some contour shapes were not precisely replicable (figure 9). A uniform area of study is required for comparison across years to more precisely evaluate changes to strata thickness and composition. The selected BSF boundary defining the edges of the salt crust is the perimeter mapped in 2003 (White and Terrazas, 2006), but modified to end at the southernmost, northernmost, and easternmost data points as there are no additional data points to constrain interpolated values beyond the edge of the data. This decision omits a small triangular wedge adjacent to I-80 and a small northeastern section that are beyond the boundaries of the measured thickness data. The area used in this study (the modified 2003 area) encompasses 95.25 km². The estimated volume of the small triangular wedge between the southern data boundary and I-80 represents ~4% of the total salt crust volume in 2003. This minor difference illustrates the impact that methodological differences and mapping approaches can introduce into calculated total salt crust volume (table 1). All change comparisons between 2003 and 2016 are based upon our recalculated 2003 volumes and contours for consistency.

Salt Crust Stratigraphy

The salt crust stratigraphy observed in 2016 has some significant differences from what was described in 2003. These differences are the result of change through time and/or differences in sampling methods and interpretations. Spatial variations in stratigraphy were analyzed qualitatively and individual strata are seen to be discontinuous across the salt flats. Spatial heterogeneity is common in surface evaporite depositional systems (e.g., Benison and others, 2007). The discontinuous nature of the BSF saline sediments suggests a dynamic depositional history, with actively changing environments and brine chemistry over the last few thousand years. The detailed depositional and diagenetic history recorded by these sediments is the topic of ongoing research and will draw from new geologic data provided by these cores (Bernau and Bowen, 2018).

Surface elevation GPS data show that, at the time of sampling, the salt crust surface had a ~0.5 m gradient dipping towards the northwest with higher elevations along the eastern edge associated with areas of surface gypsum sand accumulation (figure 5). These data align with observations of an elongate surface pond that commonly occurs along the low area on the northwest edge of the salt flats (e.g., figures 1C and 1D). This difference in

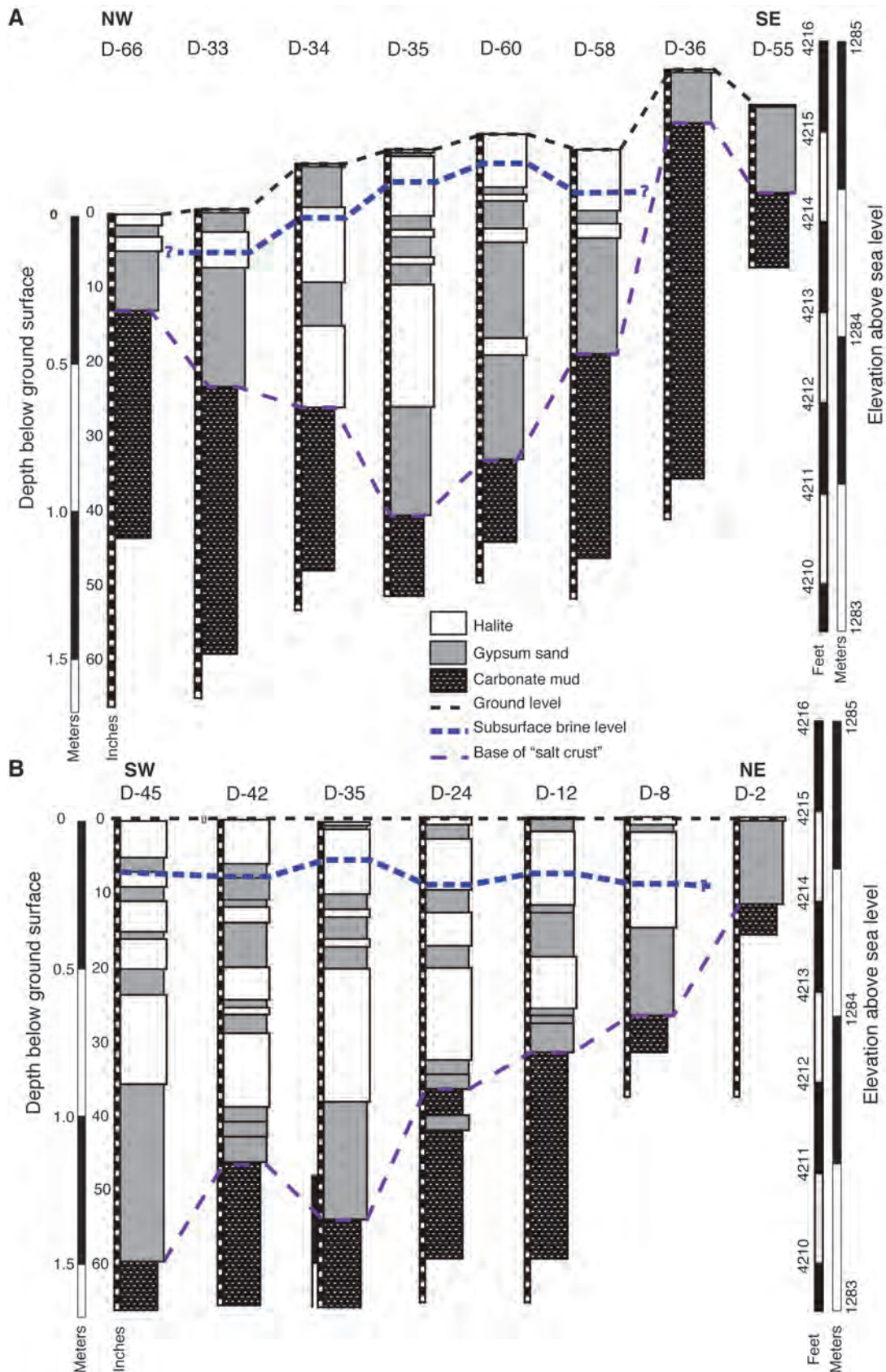


Figure 7. Example of cross-section of stratigraphic columns across BSF. Core and cross-section locations shown in figure 4. 7A shows a transect from the NW to the SE and 7B shows a transect from SW to NE. The cores are hung on the measured ground level elevation at each location. Depth to shallow brine at time of drilling (September 2016) is shown in blue dashed line. Base of total salt crust shown in purple dashed line. Stratigraphic data from all cores is included numerically in appendix A.

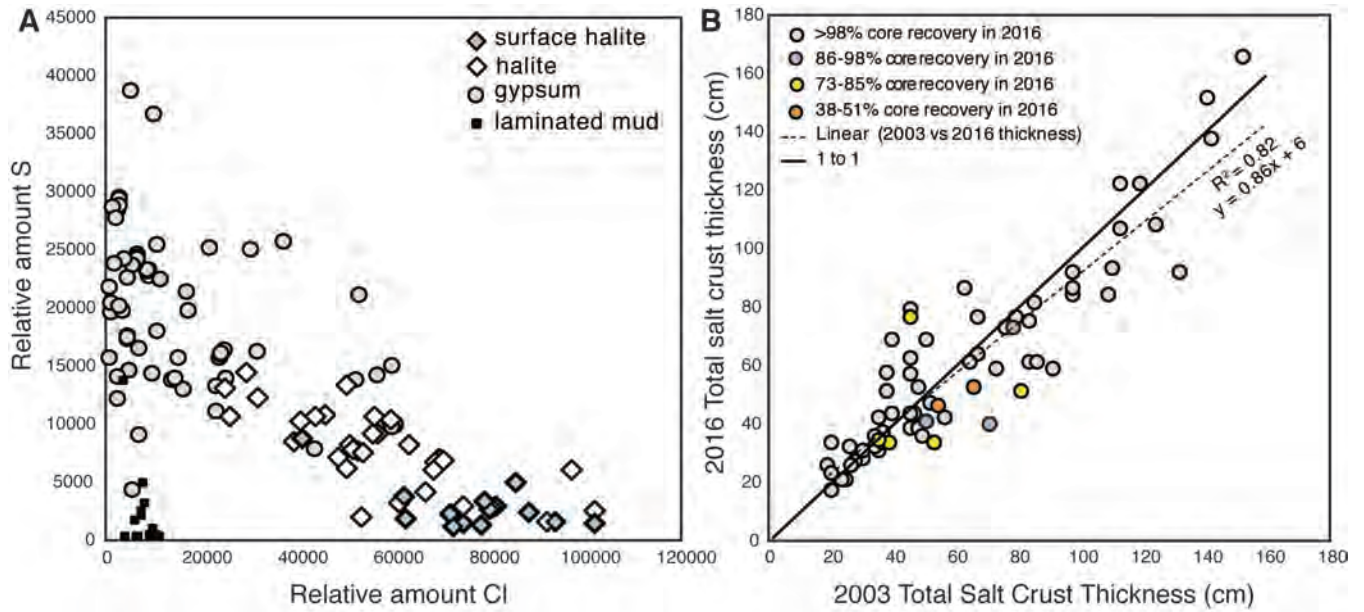


Figure 8. Comparison of total salt crust thickness measured at each site in 2003 and 2016. Sites with < 98% recovery are indicated (percent core recovery in appendix B).

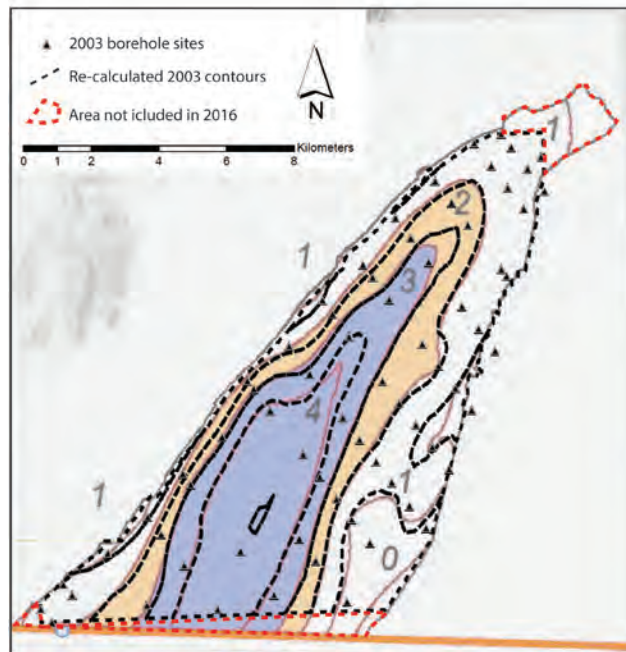


Figure 9. Comparison of kriged outputs from this study using the 2003 data vs. that published by White and Terrezas, 2006 (modified after White and Terrezas, 2006). Areas within the red dashed zones on the north and south edges were eliminated from 2016 analyses. Our recalculations using the 2003 data are used for all comparison with the 2016 data for consistency.

Table 1. Differences in 2003 salt crust thickness volume depending on area included. This study uses volume shown in method b for more direct comparison with our 2016 analyses.

2003 Salt crust volume	Method or reference	Volume (m ³)
a) GIS analysis of 2003 mud-auger measurements	See White and Terrazas (2006).	75,795,632
b) Our GIS analysis of 2003 mud-auger measurements using modified area	See methods sections of this report.	72,479,239
c) Difference between a and b	Subtraction	3,316,393
d) Estimated volume of areas not included in modified 2003 boundary used in this study	Simple volume (area * average extrapolated thickness)	3,231,526 (south) 1,426,296 (north)

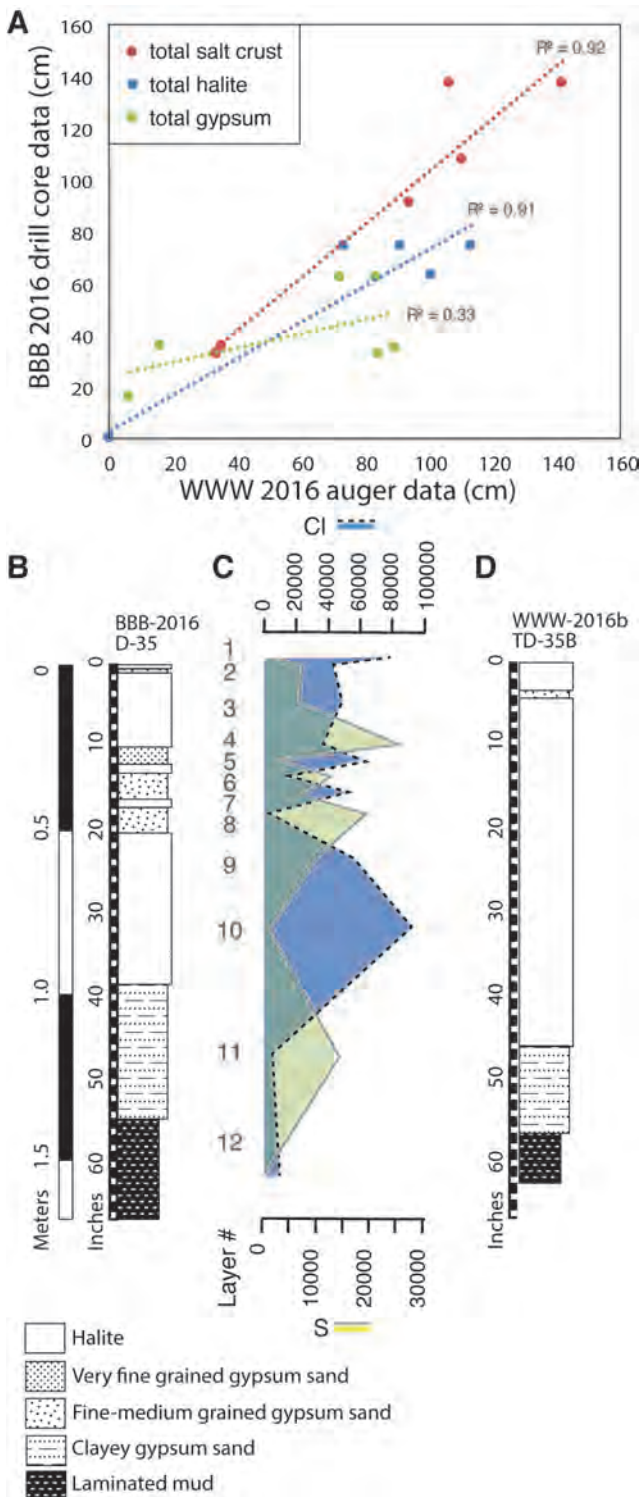


Figure 10. Comparison of core vs. auger stratigraphic observations made at same location in 2016. A) Comparison of total salt crust, total halite, and total gypsum measured by BBB (Bowen) and WWW (White) at sites D-15, D-24, D-26, D-35, and D-59 in 2016. Total salt crust results are very comparable, but there are differences in compositional observations. B) Example of stratigraphic observations at core site D-35 (A) and associated geochemical data (B) illustrating high Cl concentrations associated with halite beds and high S concentrations associated with gypsum beds. C) Stratigraphic observations from corresponding 2016 auger. Stratigraphic data in appendix B and appendix C.

ground elevation is included when comparing stratigraphy of the salt crust across the basin (figure 7), however, is not accounted for in analyses of the total salt crust thickness or in thickness of specific lithologies (e.g., halite).

At the time of the 2016 coring, W.W. White and BLM colleagues rotary-augered six sites using methods similar to those used in 2003 so that a comparison could be made between approaches (figure 10, appendix C). These comparisons show a good overall agreement between total salt crust thickness measurements ($R^2 = 0.92$), but that within that total salt crust, different interpretations were made about the presence of halite vs. gypsum (figure 10A). The Bowen team consistently measured more interbedded gypsum sand than was observed in the subsurface by the White team (figure 10B), which may be explained by the difference in sampling (rotary augering vs. straight push sonic coring). The geochemical data collected on 105 representative salt crust samples from 12 of the 2016 cores validate the mineralogical interpretations (halite vs. gypsum) made in the field and in the lab that were based on visual inspection and textures (figures 8A and 10C). The sediments described as halite are Cl-rich endmembers and the sediments described as gypsum are S-rich endmembers. However, as the geochemical data illustrate, it is not a binary system but rather a continuum with some gypsum in the halite and some halite in the gypsum. This is consistent with textural observations from cores and microscopic examination of salt crust samples (figure 3).

Some differences over time in the thickness of surface gypsum sand are to be expected, as accumulations of modern wind-blown gypsum sand are a common phenomenon on the salt flats and indeed across the West Desert of Utah. Over > 30 cm of surface gypsum sand was observed along the northeast and southwest corners of BSF that that was not present in 2003. For many of these sites it is reasonable to interpret this change as net deposition during the 13 years between studies. However, there is also a marked increase in the amount of gypsum sand observed as interbedded sediment layers in the subsurface in 2016, and there are no known reasonable processes that could have deposited subsurface gypsum sand beds during the 13 years between studies. The total and relative amounts of halite and gypsum varied considerably from 2003 to 2016 (figure 11). The total salt crust measured in 2016 was composed of ~36% halite and ~64% gypsum. In comparison, the 2003 study reported ~53% halite and 47% gypsum, which represents a 17% decrease in the relative amount of halite vs. gypsum (table 2). This difference either reflects a significant change in the composition of the salt crust over time, differences in observation linked to differing methodologies, or both. The correlation between an apparent decrease in halite with an increase

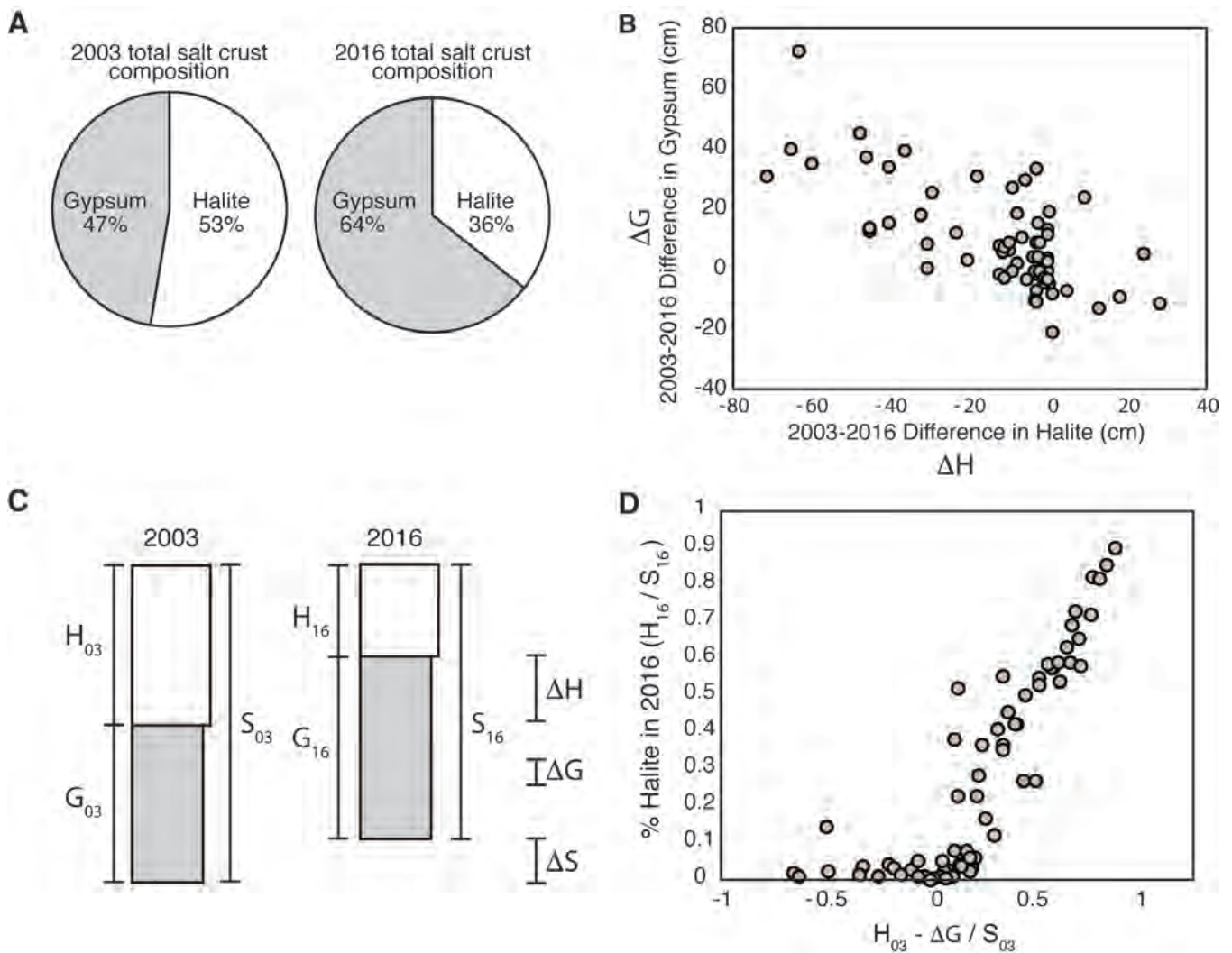


Figure 11. A) Difference in relative amount of halite and gypsum observed in 2016 and 2003 (2003 data from White and Terrazas, 2006 appendices, appendix A2). B) Comparison of difference in the amount of observed halite vs. gypsum in total salt crust in 2003 and 2016 (cm). C) Schematic illustration of salt crust stratigraphy in 2003 and 2016 and values that can be quantified and compared across studies. D) Plot of H_{03}/S_{03} versus H_{16}/S_{16} illustrating various trends in salt crust composition and relative amount of halite between the two studies.

in gypsum suggest that differences in evaporite mineral identification account for some of the observed changes through time.

The potential impact of differences in methods between 2003 and 2016 were evaluated by calculating a new metric, H^* . Calculations of H^* assume that the subsurface gypsum sand beds observed in 2016 were also present in 2003, but were either obscured by rotary-auger sampling techniques or inaccurate interpretations of evaporite mineralogy. Paired analyses between the two methods in 2016 illustrated the possibility of differential gypsum bed identification (figure 10). However, the differences in methods would not have affected the total salt crust thickness measurements (also illustrated in figure 10), only the differentiation of unconsolidated interbedded sediments within that overall thickness. H^* is the total halite measured in 2003 minus any subsurface gyp-

sum that was observed in 2016, but unaccounted for in 2003. This represents the predicted amount of total halite that would have been present in 2003 if we substitute what is described as halite with gypsum that was observed in 2016. We recognize that this is not a perfect solution to account for methodological differences, but it allows for another type of assessment of halite thickness change spatially and through time (appendix B). Calculations included the steps

$$G_{16} - G_{03} = \Delta G \quad (1)$$

$$H_{03} - \Delta G = H_{03}^* \quad (2)$$

$$H_{16} - \Delta H_{03}^* = \Delta S \quad (3)$$

where:

ΔS = change in total salt crust thickness from 2003 to 2016.

Table 2. Summary of the amounts of halite and gypsum measured in all boreholes and cores in 2003 and 2016 (n = 69).

Year	Total measured salt crust thickness (cm)	Total halite (cm)	Total gypsum (cm)	Total thickness of surface halite (cm)	% halite	% gypsum	Surface halite % of total halite
2003	4303.3	2263.7	2039.6	325.1	53%	47%	14%
2016	4119.9	1461.0	2658.9	194.8	36%	64%	13%
Difference (cm)	-183.4	-802.7	+619.3	-130.3	na	na	na
Change %	-4%	-35%	+30%	-40%	-17%	+17%	-1%

- G_{16} = gypsum measured in 2016.
- G_{03} = gypsum measured in 2003.
- ΔG = change in gypsum from 2003 to 2016.
- H_{16} = halite measured in 2016.
- H_{03} = halite measured in 2003.
- ΔH = change in halite from 2003 to 2016.
- H_{03}^* = modified 2003 halite thickness.

Analyses of H_{03}^* values relative to the total amount of salt crust in 2003 compared to the percentage of halite observed in 2016 separates the core sites where gypsum accumulated on the surface from 2003 to 2016 (negative numbers on x-axis) and the nearly one-to-one correlation between relative halite amounts for many of the cores when using H^* and accounting for missing sub-surface gypsum (figure 11D).

Spatial Variations in Salt Crust Morphology

The overall pattern of the BSF salt crust thickness observed in 2016 is similar to that seen in 2003, with the thickest strata in 2016 being 1.65 m (65 in) thick within the center of the Salduro Loop berm and extending in a SW-NE trending elongate oval that thins outward (figures 6). The distributed point measurements were gridded into continuous raster surfaces to facilitate more detailed comparison between the 2003 and 2016 studies. Subtracting the two surfaces shows that there are distinct spatial trends in the locations of observed changes, with the total salt crust thinning the most along the NW boundary (figure 12). This zone of thinning largely corresponds with the topographic low along the NW boundary and also generally correlates with the location of the historic Bonneville Speedway. In contrast, the locations with increasing total thickness over time are focused along the SW and NE corners and are associated with surface gypsum sand accumulation.

The total amount of halite observed in 2016 (summing all halite beds throughout the total salt crust thickness) shows a maximum thickness of 0.75 m (29.5 in) with the thickest sections occurring within, and just to the north-

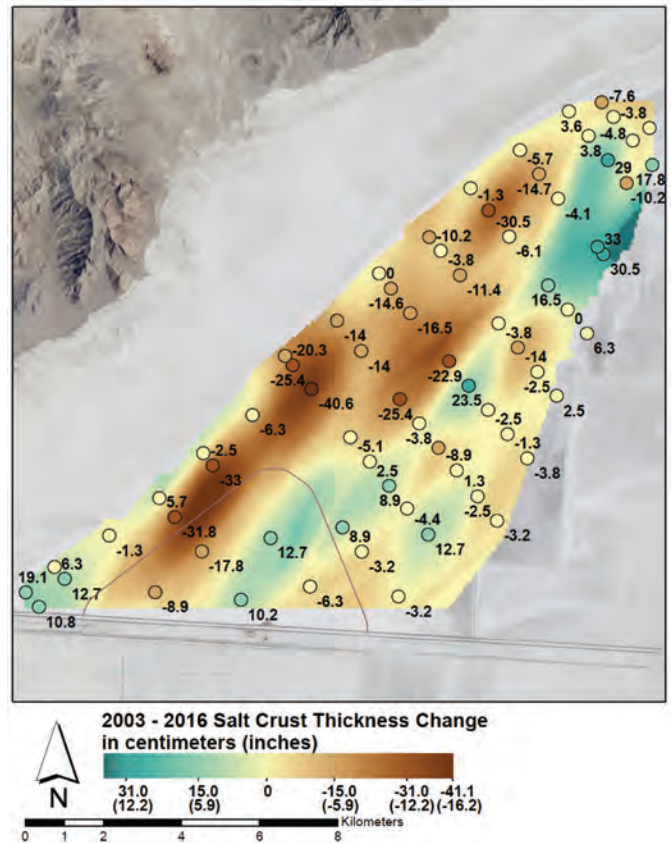


Figure 12. Spatial gridded interpolation of difference between 2003 and 2016 total salt crust thickness (decrease in thickness over time is brown, no change is yellow, increase is green).

east, of the Salduro Loop. The differences in observed total halite thickness between 2003 and 2016 illustrated that much of BSF shows a dramatic decrease in the total amount of halite that is present (figure 13), however as has been discussed, some of this apparent change is due to differences between the 2003 and 2016 studies. While halite thickness is generally seen to decrease over time, the observed thickness of gypsum generally increases between 2003 and 2016 (figure 14).

Comparing the thickness of the uppermost halite layer in 2003 (e.g., Dense Crystalline Halite in White and

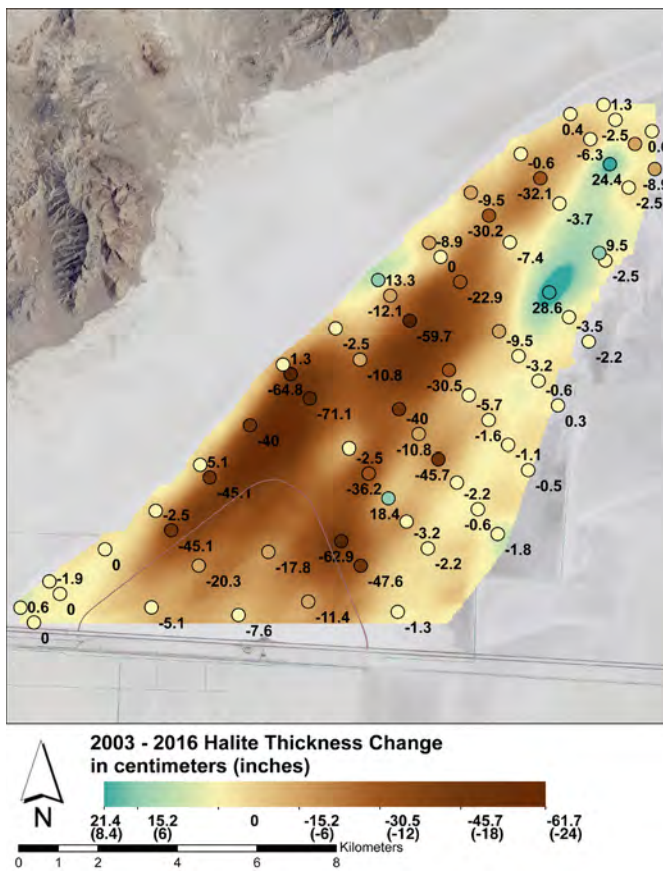


Figure 13. Spatial gridded interpolation of difference between total amount of halite measured in 2003 and 2016. Positive (green) values indicate an increase in thickness over time and negative (brown) values indicate a decrease in thickness over time.

Terrazas, 2006) to the thickness of the uppermost surface halite layer observed in 2016 shows a decrease in thickness for many sites (figure 15). A notable exception to this trend occurs within and adjacent to the Salduro Loop, where the surface halite crust layer was thicker in 2016 than in 2003. This uppermost surface halite crust changes rapidly (e.g., seasonally) and these two snapshots in time may not provide a robust assessment of long term patterns of change (Bowen and others, 2017). This change in surface halite thickness accounts for the total halite change observed at some sites (e.g., D-07, D-43, D-53).

The difference between the halite measured in 2016 and the calculated H_{03}^* values for total halite, show a similar spatial trend with decreasing halite thickness across most of BSF and the most significant change focused along the NW margin of the salt flats (figure 16). Changes in the contours of total halite between 2003 (H_{03}^*) and 2016 suggest that halite loss has occurred along the northwestern boundary of BSF, transitioning the thickest halite zone farther to the southeast. Subtracting H_{03}^* from the total halite in 2016 (figures 16A and 16B) results in the total salt crust thickness difference values (figure 12). This mathematical relationship can be

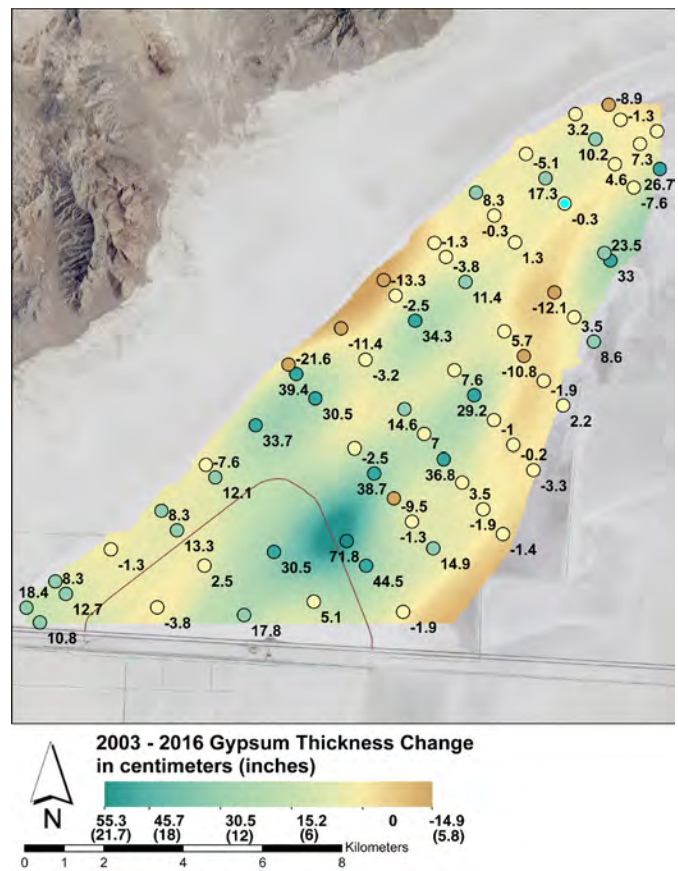


Figure 14. Spatial gridded interpolation of change in total thickness of gypsum sand measured between 2003 and 2016. Positive (green) values indicate an increase in thickness over time, and negative (brown) values indicate a decrease in thickness over time.

explained by examining the salt crust variables illustrated in figure 11C together with equations (1), (2), and (3).

Processes Driving Changes

The observations of surface relief dipping towards the northwest and the lateral changes in salt crust stratigraphy suggest that the evaporite sediments in the BSF basin may be impacted by neotectonic vertical displacement and other post-depositional changes including human land use. The downward slope of the salt crust towards the west is directionally consistent with observed deformation (“isostatic rebound”) in the Bonneville basin associated with the removal of the water from Pleistocene Lake Bonneville (Crittenden, 1963). This morphology may also be indicative of a normal fault bounding the Silver Island Mountains along the northwest boundary of BSF, which is a common feature at basin and range contacts across the region. In addition, the extraction of groundwater is known to generate land subsidence and sediment compaction, particularly in unconsolidated sedimentary systems (Galloway and Burbey, 2011).

Observed lowering of the water table at BSF (Kipnis and

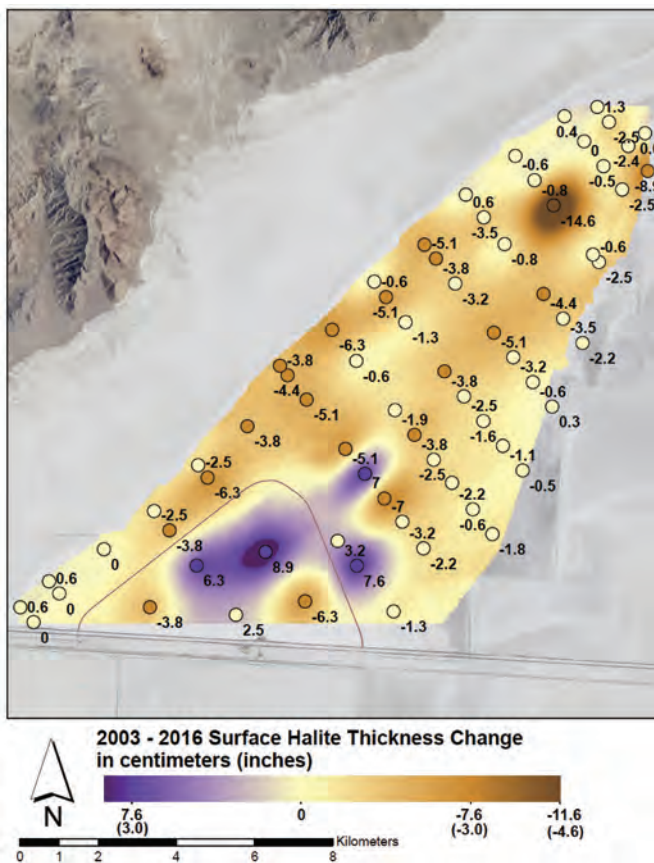


Figure 15. Spatial gridded interpolation of change in thickness of uppermost top layer of halite (“Dense Crystalline Halite” as per White and Terrazas, 2006) between 2003 and 2016. Positive (purple) values indicate an increase in thickness over time and negative (brown) values indicate a decrease in thickness over time.

Bowen, 2018) suggests that this mechanism may be a possible driver of observed changes in the volume and morphology of the BSF salt crust. Furthermore, subsurface dissolution and/or growth of evaporite minerals (e.g., displacive subsurface halite) could lead to changes both spatially and over decadal time scales in the observed order and thickness of saline strata. It is also possible that some of the observed differences are due to the dynamics of the specific season when sampling occurred, as surface halite can grow on meter per year time scales under appropriate geochemical and climatological conditions (Benison and others, 2007). The studies compared here were both conducted at the end of the evaporative season before fall rain occurred (early October in 2003 and early September in 2016), under generally similar salt crust conditions (e.g., similar extent and accessibility).

This work presents a detailed evaluation of the morphology and composition of the salt crust and evaluates how it has changed through time. However, analysis of why these changes are occurring, and the specific processes that are impacting the various observed changes are beyond the scope of this work and the focus of ongoing

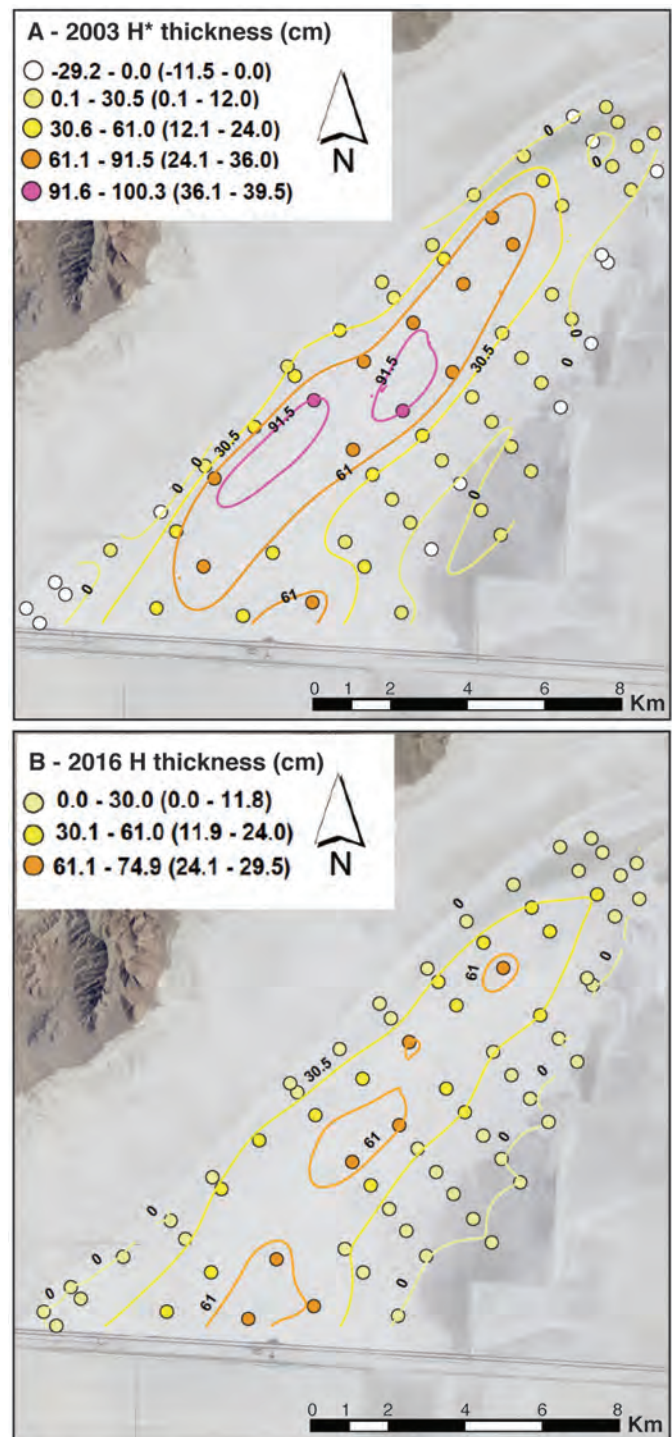


Figure 16. Contour maps of total halite based on A) recalculated 2003 total halite thickness (H^*) and B) total halite thickness measured in 2016.

research. BSF has experienced over a century of extraction and intensive land-use during a time period that has also experienced changes in hydrologic processes, temperature, and seasonality of precipitation (e.g., Bowen and others, 2017). Thus, the observation of change in this uniquely dynamic landscape may be expected. Additional ongoing research combines these salt crust thickness results with analyses of surface processes,

Table 3. Estimated total salt crust volume from 2003 and 2016 calculated using a constant surface area (modified 2003 boundary = 95.25 km²) and GIS interpolation (as described in [Appendix E](#)). One acre-foot is equivalent to 1,233.5 cubic meters.

Year	GIS-derived volume (m ³)	GIS-derived volume (acre feet)
2003	72,479,239	58,760
2016	67,464,024	54,694
% Change from 2003 to 2016	-7%	
Average % change per year	0.5% per year	

depositional history, geochemical evolution of BSF brines, microbial ecology, and the role of human extraction, mitigation, and land use to test hypotheses about the role of various “natural” and anthropogenic drivers in changing the BSF landscape. In addition, collaborations with interdisciplinary partners examine the role of social dynamics, media, and art in shaping perceptions about BSF and the importance of stakeholder communication to promote sustainable management of this unique landscape.

CONCLUSIONS

This research represents the fifth sequential “salt crust thickness study” following the work in 1960, 1973, 1988, 2003, and now 2016 (Brooks, 1991; McMillan, 1974; White and Terrazas, 2006). As with past studies, this work identified challenges with comparing across methodological differences and helped to further advance understanding of BSF salt crust dynamics. Multiple approaches have been applied towards measuring and calculating the total salt crust volume over these decadal time scales, and various methods with improvements in sampling and analytical technologies and increasing geostatistical sophistication through time. It is clear that for volume estimates of BSF to be comparable, they must be based on analyses over a static aerial footprint. Comparing our GIS-derived volume estimates from 2016 data to our re-calculation of total volume from the 2003 measurements shows a ~7% volume loss over 13 years (table 3). A simple (but less mathematically and statistically robust) volume estimate can be made by multiplying the average thickness by the area being considered, as was done in 1960, 1974, and 1988 (prior to use of GIS analysis). This approach estimates a smaller total volume, but also shows a decrease of ~8% volume from 2003 to 2016. This work demonstrates that total volume calculations and compositional interpretations are sensitive to changing field methods and data processing methods and should not be solely relied upon for accurate understanding of changes in the BSF salt crust. Spatial patterns of change are more informative than total volume comparison for evaluating the changing salt crust dynamics.

Differences in observed salt crust composition (halite vs. gypsum) are seen with different methods, and coring appears to provide a more complete record of internal stratification compared to rotary augering. Future studies aimed at measuring and characterizing changes in the composition of BSF should focus on changes in halite thickness and carefully account for interbedded gypsum. Sampling cores allows for laboratory analyses to verify, calibrate, and quantify salt crust composition and textures. The coring approach for characterizing and interpreting changes in the salt crust is very valuable and will lead to extensive additional understanding of BSF history. However, use of a sonic drill rig also presents challenges in this environment. Additional coring methods should be investigated and considered in the future (e.g., closed casing percussion cores, methods that involve freezing subsurface brine with liquid N₂, and others).

While the surface footprint of halite at BSF is dynamic and changes rapidly, that surface halite is commonly a thin veneer and does not represent the total salt crust area that links to the volume of evaporitic sediments below the surface. In addition, the location of specific isopachs or contours changes through time if the overall salt crust changes. Many of the sites we were required to sample as per the BLM-approved Intrepid Potash Mine and Reclamation Plan, contained no subsurface halite, and we question the value of coring or augering the sites around the perimeter of BSF given the time, cost, and impact of making those measurements in this highly sensitive and halite-poor environment. Finally, additional (and ongoing) research is needed to fully understand drivers of the observed changes in the BSF salt crust through time.

ACKNOWLEDGMENTS

Field and laboratory assistance was provided by multiple University of Utah students including co-author Evan Kipnis, Jeremiah Bernau, Jory Lerback, Hannah Stinson, Lily Wetterlin, Amanda Jayo, Candace Penrod, Olivia Watkins and Johns Hopkins University graduate student

Tianqui Liu. Thanks is given to Betsy Kleba for field assistance and for initiating our research on the Bonneville Salt Flats. Acknowledgment is given to co-author Jessie Pechmann for assistance with mapping and sharing GIS expertise. This work was made possible with the support of the staff of the BLM West Desert District office including Kevin Oliver, Matt Preston, Mike Nelson, Cheryl Johnson, Steve Allen, and Roxanne Tea. In addition, the support of Intrepid Potash, particularly including Eric Rogers, Craig Peterson, and Russ Draper, was essential for the success of this project. William W. White, Stan Perks, and Janice MaChipiness from the BLM are thanked for field time augering to allow for comparisons of past and current methods. The racing community, particularly Louise Noeth, William Lattin, Dennis Sullivan, and Larry Volk are acknowledged for cooperation and conversations on the salt and for donating cones and photo-reactive dye to identify drill locations during field work. Several formal and informal reviewers including William W. White, Stan Perks, Craig Peterson, Paul Jewell, Kathleen Benison, Stacey Leichliter, Weihong Wang, and Dan Stephen are acknowledged for providing feedback on drafts that improved the clarity of this work.

REFERENCES

- Benison, K.C., Bowen, B.B., Oboh-Ikuenobe, F.E., LaClair, D.A., Jagniecki, E.A., Story, S.L., Mormile, M.R., and Hong, B.Y., 2007, Sedimentology of acid saline lakes in southern Western Australia—newly described processes and products of an extreme environment: *Journal of Sedimentary Research*, v. 77, p. 366-388.
- Bernau, J.A., and Bowen, B.B., 2018, Deposition and diagenesis of the Bonneville Salt Flats [abs.]: American Association of Petroleum Geologists Annual National Meeting, Salt Lake City, Utah.
- Bowen, B.B., Kipnis, E.L., and Raming, L.W., 2017, Temporal dynamics of flooding, evaporation, and desiccation cycles and observations of salt crust area change at the Bonneville Salt Flats, Utah: *Geomorphology*, v. 299, p. 1-11.
- Brooks, S., 1991, A comparison of salt thickness on the Bonneville Salt Flats, Tooele County, Utah during July 1960, October 1974, and October 1988: Bureau of Land Management Technical Memorandum.
- Crittenden, M.D., 1963. New data on the isostatic deformation of Lake Bonneville: U.S. Geological Survey Professional Paper 454-E, p. E1-E31.
- Galloway, D. L., and Burbey, T. J., 2011, Review—regional land subsidence accompanying groundwater extraction: *Hydrogeology Journal*, v. 19, p. 1459–1486.
- Kipnis, E.L. and Bowen, B.B., 2018, Salt crust change and humans as geologic agents, *in* Emerman, S.H., Bowen, B.B., Schamel, S., and Simmons, S., editors, Utah Geological Association Publication 47—Geofluids of Utah, this volume.
- Lowenstein, T. K., and Hardie, L. A., 1985, Criteria for the recognition of salt-pan evaporites: *Sedimentology*, v. 32, no. 5, p. 627-644 (doi:10.1111/j.1365-3091.1985.tb00478.x).
- Mason, J. and Kipp, K., 1998, Hydrology of the Bonneville Salt Flats, northwestern Utah, and simulation of ground-water flow and solute transport in the shallow-brine aquifer: U.S. Geological Survey Professional Paper 1585, 108 p.
- McMillan, D. T., 1974, Bonneville Salt Flats: A Comparison of Salt Thickness in July, 1960 and October, 1974. Utah Geological and Mineral Survey Report of Investigation No. 91, 4 maps, 6 p.
- Noeth, L. A., 2002, Bonneville—the fastest place on Earth: St. Paul, Minnesota, MBI Publishing Company, 156 p.
- Nolan, T.B., 1928, Potash brines in the Great Salt Lake Desert, Utah, *in* Loughlin G.F., and Mansfield, G.R., editors, Contributions to Economic Geology, Part I—Metals and Nonmetals except Fuels: U.S. Geological Survey Bulletin, v. 795, p. 25-44.
- Oviatt, C. G., 2015, Chronology of Lake Bonneville, 30,000 to 10,000 yr B.P.: *Quaternary Science Reviews*, v. 110, p. 166-171.
- U.S. Bureau of Land Management West Desert District, 2012, Intrepid Potash Mine and Reclamation Plan Environmental Analysis and Decision Record (EA #UT-020-2006-002, August and September 2012).
- White, W.W., 2004, Replenishment of salt to the Bonneville Salt Flats—results of the five-year experimental Salt Laydown Project, *in* Castor, S.B., Papke, K.G., and Meeuwig, R.O., editors, Betting on industrial minerals, Proceedings of the 39th Forum on the Geology of Industrial Minerals: Reno/Sparks, Nevada, Nevada Bureau of Mines and Geology Special Publication 33, p. 243-262.
- White, W.W. and Terrazas, M., 2006, Analysis of recent and historical salt-crust thickness measurements and assessment of their relationship to the salt laydown project, Bonneville Salt Flats, Tooele County, Utah, *in* Harty, K.H., and Tabet, D.E., editors, Geology of northwest Utah: Utah Geological Association Publication 34, p. 272-302.

APPENDICES**Appendix A.** Summary of 2016 core recovery**Table A-1.** Percent core recovery for cores with <98% recovery.

Core #	% recovery
D-10	78
D-13	75
D-14	73
D-19	95
D-21	38
D-28	80
D-31	54
D-37	86
D-44	98
D-62	93
D-66	73
D-71	79

Appendix B. Core data collected and used in this study**Table B-1.** Core locations (latitude and longitude in UTM) and summary of total stratigraphic data (in inches) including total 2016 salt crust thickness, total core thickness, total amount of measured halite, and total amount of measured gypsum per core.

Core ID	Longitude UTM E	Latitude UTM N	Total 2016 salt crust thickness (in)	Total 2016 core thickness (in)	Total 2016 measured halite (in)	Total 2016 measured gypsum (in)
D-2	268978.89	4526512.3	12	16	0.5	11.5
D-3	267755.56	4527184.52	15	18.5	1.0	14.0
D-4	268054.98	4526801.68	17	17.5	0.5	16.5
D-5	268547.04	4526187	18.5	22	0.5	18.0
D-6	269051.13	4525548.17	27	36	1.0	26.0
D-7	266914.26	4526948.55	17	19	0.5	16.5
D-8	267914.59	4525672.95	27	32	14.0	13.0
D-9	268391.37	4525076.46	15	19	0.5	14.5
D-10	265657.75	4525934.81	13	46.5	1.0	12.0
D-11	266150.26	4525315.25	23	60	14.5	8.5
D-12	266637.08	4524670.25	32	60	17.3	14.8
D-13	267797.71	4523219.96	30	60	0.5	29.5
D-14	264852.5	4524365.65	20	44	18.0	2.0
D-15	265383.25	4523683.26	36	60	29.5	6.5
D-16	266378.76	4522409.64	24.5	60	13.5	11.0
D-17	266880.06	4521778.82	14.5	15.5	0.1	14.4
D-18	267376.11	4521155.48	10	30	0.1	9.9
D-19	263336.5	4523667.59	16	57	1.0	15.0
D-20	265111.41	4521419.42	25	37	10.5	14.5
D-21	265604.77	4520788.24	20.5	22.5	0.5	20.0
D-22	266106.07	4520157.42	11	21	0.3	10.8
D-23	262352.54	4522327.37	16.5	32.5	2.0	14.5
D-24	262848.7	4521688.18	42.5	60	25.0	14.0
D-25	263845.28	4520429.16	24	60	20.5	3.5
D-26	264843.95	4519159.1	13	30	0.1	12.9
D-27	265339.22	4518530.3	10.5	12.5	0.1	10.4
D-28	260973.73	4521494.42	14	48	7.5	6.5
D-29	261589.23	4520696.48	33	60	19.0	14.0
D-30	262578.58	4519440.14	33	49	27.0	6.0
D-31	263572.55	4518175.72	18	32.5	3.0	15.0
D-32	264571.93	4516908.69	12.5	16.5	1.0	11.5
D-33	259833.75	4520329.35	24	60	6.5	17.5
D-34	260320.15	4519709.37	36	60	23.5	12.5
D-35	261313.67	4518449.85	54	84	29.5	24.5
D-36	262768.62	4516590.66	8	60	0.5	7.5
D-37	258806.53	4519028.32	28.5	51.5	15.0	13.5
D-38	261606.18	4515467.17	30	60	11.0	19.0
D-39	262545.79	4514295.37	6.75	18	0.3	6.5
D-41	257785.1	4517717.96	23	36	16.5	6.5

D-42	259271.78	4515821.17	65	67	26.5	38.5
D-43	256419.07	4516865.08	12.5	60	0.5	12.0
D-44	256811.82	4516368.25	15.5	56.5	9.0	6.5
D-45	258512.81	4514211.49	59.5	59.5	27.0	32.5
D-46	255138.12	4515888.11	10	21	0.5	9.5
D-48	253730.47	4515068.88	16.5	16.5	0.5	16.0
D-49	253993.66	4514754.9	20	33	0.3	19.8
D-50	252997.41	4514403.12	22.5	30.5	0.5	22.0
D-51	253336.11	4514024.25	22.25	31.25	0.3	22.0
D-52	256311.85	4514408.74	29.5	60.5	17.0	12.5
D-53	260277.94	4514556.36	42	60	24.5	17.5
D-54	257507.71	4515471.38	36.5	60	21.5	15.0
D-55	263308.04	4515912.26	13	24	0.1	12.9
D-56	261114.04	4516098.32	48	60	11.0	37.0
D-57	265073.15	4516275.43	8	10.5	0.1	7.9
D-58	262309.35	4517181.71	30	60	11.0	19.0
D-59	264040.96	4517584.38	14	24	0.1	13.9
D-60	261811.22	4517816.09	48	60	13.5	34.5
D-61	265843.57	4517899.38	13	15	0.1	12.9
D-62	257546.45	4518036.65	17	56	6.0	11.0
D-63	263076.13	4518806.39	28.5	66	12.0	16.5
D-64	266600.14	4519529.26	9	15	0.1	8.9
D-65	264345.8	4519792.88	34	60	13.0	21.0
D-66	259637.77	4520571.04	13	43.5	3.5	9.5
D-67	264122.08	4522676.37	34	60	23.5	10.5
D-68	262049.9	4522723.73	12	60	6.0	6.0
D-69	263630.1	4523312.39	24	60	17.5	6.5
D-70	267644.08	4523412.73	31	60	4.5	26.5
D-71	264392.92	4524946.95	13.5	48.5	0.0	13.5
D-72	267416.49	4526308.55	20.5	25	1.0	19.5

Table B-2. Summary of 2003 measurements used in comparisons (after White and Terrazas, 2006).

Core ID	Total 2003 Salt Crust thickness (in)	Total 2003 measured halite (in)	Total 2003 measured gypsum (in)	2003 surface halite thickness (DCH) (in)
D-2	14	0.25	13.75	0.25
D-3	18	0.5	17.5	0.5
D-4	18.5	1.5	17	1.5
D-5	20.4	5.28	15.12	1.44
D-6	20	4.5	15.5	4.5
D-7	15.6	0.36	15.24	0.36
D-8	15.6	4.4	11.2	1.2
D-9	19	1.5	17.5	1.5
D-10	15.25	1.25	14	1.25
D-11	28.8	27.12	1.68	1.32
D-12	33.6	18.72	14.88	6
D-13	18	1.5	16.5	1.5
D-14	32	29.88	2.13	2.38
D-15	38.4	32.4	6	1.8
D-16	18	2.25	15.75	2.25
D-17	14.5	1.5	13	1.5
D-18	7.5	1	6.5	1
D-19	20	4.5	15.5	3
D-20	26.5	14.25	12.25	2.5
D-21	26	1.75	24.25	1.75
D-22	12	0.5	11.5	0.5
D-23	22.25	6.75	15.5	3
D-24	49	48.5	0.5	1.5
D-25	33	32.5	0.5	2
D-26	14	0.75	13.25	0.75
D-27	11	0.5	10.5	0.5
D-28	19.5	8.5	11	3.5
D-29	38.5	23.25	15.25	1.25
D-30	43	42.75	0.25	2.25
D-31	21.5	21	0.5	2
D-32	13.5	1.25	12.25	1.25
D-33	34	32	2	3.25
D-34	52	51.5	0.5	2.5
D-35	56	30.5	25.5	2.5
D-36	9.75	1.75	8	1.75
D-37	31	30.75	0.25	3.5
D-38	31.25	29.75	1.5	4
D-39	8	0.75	7.25	0.75
D-41	36	34.25	1.75	3
D-42	60	33.5	26.5	2.5
D-43	10.25	1.5	8.75	1.5
D-44	28	26.75	1.25	2.5

D-45	55.5	30	25.5	4
D-46	10.5	0.5	10	0.5
D-48	14	1.25	12.75	0.25
D-49	15	0.25	14.75	0.25
D-50	15	0.25	14.75	0.25
D-51	18	0.25	17.75	0.25
D-52	33	19	14	2.5
D-53	44.5	29	15.5	4
D-54	43.5	29.5	14	1
D-55	8	1	7	1
D-56	44.5	35.75	8.75	3.75
D-57	9.25	0.75	8.5	0.75
D-58	26.5	3.75	22.75	3.75
D-59	13.5	1	12.5	1
D-60	47	27.75	19.25	3.25
D-61	14.5	0.25	14.25	0.25
D-62	18	4	14	4
D-63	30	16.25	13.75	2.5
D-64	8	0	8	0
D-65	24.75	15.25	9.5	1.5
D-66	21	3	18	3
D-67	38.5	32.5	6	1.75
D-68	12	0.75	11.25	0.75
D-69	25.5	17.5	8	2
D-70	18	0.75	17.25	0.75
D-71	14	3.75	10.25	0.25
D-72	19	3.5	15.5	1

Table B-3. Stratigraphic measurements from 2016 core analyses. The nomenclature from White and Terrazas (2006) are used to distinguish strata. DCH = dense crystalline halite, CPH = coarse porous halite, GYP = gypsum, LAH = loose aggregated halite, CLAY = laminated carbonate mud. Layers are numbered so that each core has sequential numbering of unique strata corresponding with observations from the top (ground surface) down.

Core ID (number of stratigraphic layers in salt crust at that location)	Sediment type-layer number	Thickness (in)
D-2 (2)	DCH-1	0.5
	GYP-2	11.5
D-3 (3)	DCH-1	1.0
	GYP-2	11.0
	GYP-3	3.0
D-4 (3)	DCH-1	0.5
	GYP-2	11.5
	GYP-3	5.0
D-5 (2)	DCH-1	0.5
	GYP-2	18.0
D-6 (2)	DCH-1	1.0
	GYP-2	26.0
D-7 (2)	DCH-1	0.5
	GYP-2	16.5
D-8 (4)	DCH-1	1.0
	GYP-2	1.0
	CPH-3	13.0
	GYP-4	12.0
D-9 (2)	DCH-1	0.5
	GYP-2	14.5
D-10 (3)	DCH-1	1.0
	GYP-2	12
	CLAY-4	1.5
D-11 (7)	DCH-1	1.0
	GYP-2	1.5
	LAH-3	8.0
	GYP-4	3.5
	GYP-5	3.0
	CPH-6	5.5
	GYP-7	0.5
D-12 (9)	DCH-1	0.25
	GYP-2	1.75
	LAH-3	10.0
	GYP-4	1.0
	GYP-5	6.0
	LAH-6	7.0
	GYP-7	1.0
	GYP-8	1.0
	GYP-9	4.0

D-13 (3)	DCH-1	0.5
	GYP-2	0.5
	GYP-3	29.0
D-14 (4)	DCH-1	1.0
	GYP-2	2.0
	CPH-3	15.0
	LAH-4	2.0
D-15 (4)	DCH-1	1.5
	GYP-2	4.5
	LAH-3	28.0
	GYP-4	2.0
D-16 (7)	DCJ-1	0.5
	GYP-2	2.0
	LAH-3	6.5
	GYP-4	0.5
	LAH-5	6.5
	GYP-6	8.0
	GYP-7	0.5
D-17 (2)	DCH-1	0.125
	GYP-2	14.275
D-18 (2)	DCH-1	0.125
	GYP-2	9.875
D-19 (3)	DCH-1	1.0
	GYP-2	12.0
	GYP-3	3.0
D-20 (7)	DCH-1	0.5
	GYP-2	3.0
	LAH-3	3.0
	GYP-4	2.0
	LAH-5	7.0
	GYP-6	5.0
	GYP-7	4.5
D-21 (3)	DCH-1	0.5
	GYP-2	15.5
	GYP-3	4.5
D-22 (2)	DCH-1	0.25
	GYP-2	10.75
D-23 (5)	DCH-1	1.0
	GYP-2	2.0
	LAH-3	1.0
	GYP-4	11.0
	GYP-5	1.5

D-24 (11)	DCH-1	1.0
	GYP-2	2.0
	LAH-3	7.0
	GYP-4	3.0
	CPH-5	4.5
	GYP-6	3.0
	LAH-7	2.5
	LAH-8	10.0
	GYP-9	2.0
	GYP-10	2.0
	GYP-11	2.0
D-25 (8)	DCH-1	0.5
	LAH-2	10.5
	GYP-3	0.5
	LAH-4	4.5
	GYP-5	1.0
	GYP-6	1.0
	LAH-7	5.0
	GYP-8	1.0
D-26 (2)	DCH-1	0.125
	GYP-2	12.875
D-27 (2)	DCH-1	0.06
	GYP-2	10.44
D-28 (5)	DCH-1	1.0
	GYP-2	0.5
	LAH-3	6.5
	GYP-4	5.0
	GYP-5	1.0
D-29 (8)	DCH-1	1.0
	CPH-2	10.0
	GYP-3	5.0
	GYP-4	2.0
	LAH-5	8.0
	GYP-6	4.0
	GYP-7	1.0
	GYP-8	2.0
D-30 (7)	DCH-1	1.5
	LAH-2	4.0
	GYP-3	4.0
	LAH-4	16.0
	GYP-5	2.0
	LAH-6	3.0
	LAH-7	2.5

D-31 (6)	DCH-1	1.5
	GYP-2	2.0
	DCH-3	1.0
	GYP-4	1.0
	DCH-5	1.0
	GYP-6	12.0
D-32 (2)	DCH-1	1.0
	GYP-2	11.5
D-33 (4)	DCH-1	1.5
	GYP-2	1.5
	LAH-3	5.0
	GYP-4	16.0
D-34 (5)	DCH-1	0.5
	GYP-2	6.0
	LAH-3	11.0
	GYP-4	6.5
	LAH-5	12.0
D-35 (11)	DCH-1	0.5
	GYP-2	0.5
	DCH-3	9.0
	GYP-4	2.0
	DCH-5	1.0
	GYP-6	3.0
	CPH-7	1.0
	GYP-8	3.0
	LAH-9	4.0
	LAH-10	14.0
	GYP-11	16.0
D-36 (3)	DCH-1	0.5
	GYP-2	1.5
	GYP-3	6.0
D-37 (8)	DCH-1	2.0
	GYP-2	4.5
	LAH-3	4.0
	GYP-4	4.0
	LAH-5	4.0
	GYP-6	1.0
	LAH-7	5.0
	GYP-8	4.0
D-38 (6)	DCH-1	7.0
	GYP-2	1.0
	CPH-3	4.0
	GYP-4	4.0
	GYP-5	2.0
	GYP-6	12.0
D-39 (2)	DCH-1	0.25
	GYP-2	6.5

D-41 (7)	DCH-1	0.5
	GYP-2	1.5
	CPH-3	9.0
	GYP-4	2.0
	LAH-5	5.0
	GYP-6	3.0
	LAH-7	2.0
D-42 (14)	DCH-1	6.0
	GYP-2	2.0
	LAH-3	3.0
	GYP-4	1.0
	CPH-5	2.0
	GYP-6	4.0
	GYP-7	2.0
	LAH-8	4.5
	GYP-9	1.0
	CPH-10	1.0
	GYP-11	2.5
	LAH-12	10
	GYP-13	24
	GYP-14	2.0
D-43 (2)	DCH-1	0.5
	GYP-2	12.0
D-44 (4)	DCH-1	1.0
	GYP-2	4.0
	LAH-3	8.0
	GYP-4	2.5
D-45 (11)	DCH-1	5.0
	GYP-2	2.0
	CPH-3	2.0
	GYP-4	2.0
	CPH-5	4.0
	GYP-6	1.0
	LAH-7	4.0
	GYP-8	3.5
	LAH-9	6.0
	LAH-10	6.0
	GYP-11	24.0
D-46 (2)	DCH-1	0.5
	GYP-2	9.5
D-48 (3)	DCH-1	0.5
	GYP-2	14.5
	GYP-3	1.5
D-49 (3)	DCH-1	0.25
	GYP-2	18.75
	GYP-3	1.0

D-50 (3)	DCH-1	0.5
	GYP-2	20.0
	GYP-3	2.0
D-51 (2)	DCH-1	0.25
	GYP-2	22.0
D-52 (9)	DCH-1	1.0
	GYP-2	1.0
	LAH-3	6.0
	GYP-4	4.0
	LAH-5	5.0
	GYP-6	1.0
	LAH-7	5.0
	GYP-8	1.5
	GYP-9	5.0
D-53 (7)	DCH-1	1.5
	LAH-2	7.0
	GYP-3	3.5
	CPH-4	3.0
	GYP-5	4.0
	LAH-6	13.0
	GYP-7	10.0
D-54 (9)	DCH-1	3.5
	GYP-2	2.0
	LAH-3	5.0
	GYP-4	5.5
	LAH-5	4.0
	GYP-6	5.0
	LAH-7	5.0
	LAH-8	4.0
	GYP-9	2.5
D-55 (2)	DCH-1	0.125
	GYP-2	12.875
D-56 (5)	DCH-1	5.0
	GYP-2	2.0
	GYP-3	24.0
	LAH-4	6.0
	GYP-5	11.0
D-57 (2)	DCH-1	0.06
	GYP-2	7.94
D-58 (6)	DCH-1	1.0
	CPH-2	8.0
	GYP-3	2.0
	CPH-4	2.0
	GYP-5	15.0
	GYP-6	2.0
D-59 (2)	DCH-1	0.125
	GYP-2	13.875

D-60 (11)	DCH-1	6.0
	LAH-2	2.0
	GYP-3	1.0
	LAH-4	1.0
	GYP-5	4.0
	CPH-6	2.0
	GYP-7	14.0
	CPH-8	2.5
	GYP-9	12.0
	GYP-10	1.0
	GYP-11	2.5
D-61 (2)	DCH-1	0.06
	GYP-2	12.94
D-62 (4)	DCH-1	3.0
	GYP-2	2.0
	CPH-3	3.0
	GYP-4	9.0
D-63 (11)	DCH-1	1.0
	GYP-2	2.0
	LAH-3	2.0
	GYP-4	1.5
	LAH-5	1.0
	GYP-6	2.0
	CPH-7	4.0
	GYP-8	2.0
	LAH-9	4.0
	GYP-10	7.0
	GYP-11	2.0
D-64 (11)	CPH-1	1.0
	GYP-2	2.0
	LAH-3	2.0
	GYP-4	1.5
	LAH-5	1.0
	GYP-6	2.0
	CPH-7	4.0
	GYP-8	2.0
	LAH-9	4.0
	GYP-10	7.0
	GYP-11	2.0

D-65 (11)	DCH-1	1.0
	GYP-2	2.0
	LAH-3	2.0
	GYP-4	1.5
	LAH-5	1.0
	GYP-6	2.0
	CPH-7	4.0
	GYP-8	2.0
	LAH-9	4.0
	GYP-10	7.0
	GYP-11	2.0
D-66 (5)	DCH-1	1.5
	GYP-2	1.5
	LAH-3	2.0
	GYP-4	7.0
	GYP-5	1.0
D-67 (8)	DCH-1	0.5
	CPH-2	1.0
	GYP-3	0.5
	LAH-4	14.0
	GYP-5	1.0
	LAH-6	8.0
	GYP-7	3.0
	GYP-8	6.0
D-68 (5)	DCH-1	0.5
	LAH-2	1.5
	GYP-3	2.0
	LAH-4	4.0
	GYP-5	4.0
D-69 (7)	DCH-1	0.5
	GYP-2	2.0
	LAH-3	0.5
	GYP-4	2.0
	LAH-5	0.5
	GYP-6	2.5
	LAH-7	16.0
D-70 (5)	DCH-1	0.5
	GYP-2	3.0
	LAH-3	4.0
	GYP-4	15.5
	GYP-5	8.0
D-71 (2)	DCH-1	0.5
	GYP-2	13.0
D-72 (3)	DCH-1	1.0
	GYP-2	15.5
	GYP-3	4.0

Table B-4. Salt crust thickness values calculated from 2003 and 2016 measurements.

Core ID	Difference in total salt crust thickness in inches (2003-2016)	ΔG in inches (total gypsum in 2003 – total gypsum in 2016)	ΔH in inches (total halite in 2003 – total halite in 2016)	Difference in uppermost surface halite layer in inches (DCH 2003 – DCH 2016)	$H_{03}^* (H_{03} - \Delta G)$
D-2	-2	2.3	-0.3	0.25	2.5
D-3	-3	3.5	-0.5	0.5	4
D-4	-1.5	0.5	1.0	-1	2
D-5	-1.9	-2.9	4.8	-0.94	2.4
D-6	7	-10.5	3.5	-3.5	-6
D-7	1.4	-1.3	-0.1	0.14	-0.9
D-8	11.4	-1.8	-9.6	-0.2	2.6
D-9	-4	3.0	1.0	-1	4.5
D-10	-2.25	2.0	0.3	-0.25	3.25
D-11	-5.8	-6.8	12.6	-0.32	20.3
D-12	-1.6	0.1	1.5	-5.75	18.6
D-13	12	-13.0	1.0	-1	-11.5
D-14	-12	0.1	11.9	-1.38	30.01
D-15	-2.4	-0.5	2.9	-0.3	31.9
D-16	6.5	4.8	-11.3	-1.75	7
D-17	0	-1.4	1.4	-1.375	0.125
D-18	2.5	-3.4	0.9	-0.875	-2.375
D-19	-4	0.5	3.5	-2	5
D-20	-1.5	-2.3	3.8	-2	12
D-21	-5.5	4.3	1.3	-1.25	6
D-22	-1	0.8	0.3	-0.25	1.25
D-23	-5.75	1.0	4.8	-2	7.75
D-24	-6.5	-13.5	23.5	-0.5	35
D-25	-9	-3.0	12.0	-1.5	29.5
D-26	-1	0.4	0.6	-0.625	1.125
D-27	-0.5	0.1	0.4	-0.4375	0.5625
D-28	-5.5	4.5	1.0	-2.5	13
D-29	-5.5	1.3	4.3	-0.25	24.5
D-30	-10	-5.8	15.8	-0.75	37
D-31	-3.5	-14.5	18.0	-1	6.5
D-32	-1	0.8	0.3	-0.25	2
D-33	-10	-15.5	25.5	-1.75	16.5
D-34	-16	-12.0	28.0	-2	39.5
D-35	-2	1.0	1.0	-2	31.5
D-36	-1.75	0.5	1.3	-1.25	2.25
D-37	-2.5	-13.3	15.8	-1.5	17.5
D-38	-1.25	-17.5	18.8	3	12.25
D-39	-1.25	0.8	0.5	-0.5	1.5
D-41	-13	-4.8	17.8	-2.5	29.5

D-42	5	-12.0	7.0	3.5	21.5
D-43	2.25	-3.3	1.0	-1	-1.75
D-44	-12.5	-5.3	17.8	-1.5	21.5
D-45	4	-7.0	3.0	1	23
D-46	-0.5	0.5	0.0	0	1
D-48	2.5	-3.3	0.8	0.25	-2
D-49	5	-5.0	0.0	0	-4.75
D-50	7.5	-7.3	-0.3	0.25	-7
D-51	4.25	-4.3	0.0	0	-4
D-52	-3.5	1.5	2.0	-1.5	20.5
D-53	-2.5	-2.0	4.5	-2.5	27
D-54	-7	-1.0	8.0	2.5	28.5
D-55	5	-5.9	0.9	-0.875	-4.875
D-56	3.5	-28.3	24.8	1.25	7.5
D-57	-1.25	0.6	0.7	-0.69	1.31
D-58	3.5	3.8	-7.3	-2.75	7.5
D-59	0.5	-1.4	0.9	-0.875	-0.375
D-60	1	-15.3	14.3	2.75	12.5
D-61	-1.5	1.3	0.2	-0.19	1.56
D-62	-1	3.0	-2.0	-1	7
D-63	-1.5	-2.8	4.3	-1.5	13.5
D-64	1	-0.9	-0.1	0.125	-0.875
D-65	9.25	-11.5	2.3	-1	3.75
D-66	-8	8.5	-0.5	-1.5	11.5
D-67	-4.5	-4.5	9.0	-1.25	28
D-68	0	5.3	-5.3	-0.25	6
D-69	-1.5	1.5	0.0	-1.5	19
D-70	13	-9.3	-3.8	-0.25	-8.5
D-71	-0.5	-3.3	3.8	0.25	0.5
D-72	1.5	-4.0	2.5	0	-0.5

Appendix C. 2016 comparison auger data for methodological variability assessment.

Table C-1. Salt crust stratigraphy measurements for sites D-15B, D-24, D-26, D-35, D-59 made by W.W. White and colleagues September 7 and 8, 2016 using auguring. Differences between cored (BBB) and augur-measured (WWW) values for site D-35 shown graphically in Figure 10.

CH to LAg: Transition from coarse halite to loose-aggregated halite

LAg+gyp+clay: Mix of loose-aggregated halite, gypsum (sand-size crystals), & clay matrix

STWL: Static water level – measured after ground-water level stabilized in borehole

TD: Twinned mud-auger boreholes located 6-ft north of University of Utah sonic-drilled core holes

UU-D: 2016 mud-auger boreholes (locations inaccessible for sonic drill rig)

Date	ID	DCH	1 st Gyp	CH to LAg	LAg+gyp+Clay	Total salt crust WW	Clay	TD	STWL	Total halite	Total gypsum
2016	TD-15B	0-1.0	1.0-2.0	2.0-37.0		37	37.0-42.0	42	7	36	1
2016	TD-24	0-0.75	0.75-2.0	2.0-41.0	41.0-43.5	43.5	43.5-51.5	51.5	10	39.75	2.5
2016	UU-D-26	0.0-0.125	0.125-13.25			13.25	13.25-19.0 blue	30	19	0.125	13.125
							19.0-23.0 trans				
							23.0-30.0 tan				
2016	TD-35A	0-3.0	3.0-4.0	4.0-30.0	30.0-42.0	42	42	42	4.5	29	13
2016	TD-35B	0-3.5	3.5-4.5	4.5-45.75	45.75-56.0	56	56.0-62.0	62	5	44.75	11.25
2016	UU-D-59	0.0-0.125	0.125-8.0 white			14	14.0-20.0 blue	24		0.125	13.875
			8.0-14.0 gray				20.0-24.0 tan				

Appendix D. Examples of Cl and S relative concentrations for gypsum and halite**Table D-1.** Cl and S relative concentrations reported in total photon counts from 90 seconds of pXRF (Bruker Tracer3) analysis with blue filter under He vacuum for representative 12 cores (D-2, D-8, D-12, D-24, D-33, D-34, D-35, D-42, D-45, D-55, D-60, D-66) all included in Figure 7. Multiple analyses were performed on samples from core D-12 to test precision of analyses (average standard deviation = 2 for both Cl and S).

Sample	Textural interpretation	Cl	S
D-12-01b	halite	81269	2760
D-12-01c	halite	80409	2604
D-12-01d	halite	79685	2577
D-12-02a	gypsum	8380	23018
D-12-02b	gypsum	8457	22489
D-12-02c	gypsum	8191	22850
D-12-02d	gypsum	8090	22977
D-12-03a	gypsum	60061	9656
D-12-03b	gypsum	59194	9902
D-12-03c	gypsum	60067	9766
D-12-03d	gypsum	59387	9511
D-12-04a	gypsum	23354	15533
D-12-04b	gypsum	24207	16177
D-12-04c	gypsum	23772	15805
D-12-04d	gypsum	23536	15931
D-12-05a	gypsum	5791	23566
D-12-05b	gypsum	6051	24421
D-12-05c	gypsum	6029	24058
D-12-05d	gypsum	6001	23937
D-12-06a	halite	69230	6798
D-12-06b	halite	69496	6785
D-12-06c	halite	68541	6575
D-12-06d	halite	70008	6712
D-12-07a	gypsum	4090	17072
D-12-07b	gypsum	4176	17429
D-12-07c	gypsum	4123	17270
D-12-07d	gypsum	4139	17175
D-12-08a	gypsum	2157	28176
D-12-08b	gypsum	2171	29210
D-12-08c	gypsum	2322	29118
D-12-08d	gypsum	2266	28521
D-12-09	gypsum	5242	4168
D-12-10	lam	9129	131
D-02-01	halite	61840	3565
D-02-02	gypsum	204	21511
D-02-03	lam	6003	49
D-24-01	halite	74416	1269
D-24-02	gypsum	13266	13567
D-24-03	halite	31067	12105

D-24-04	gypsum	24869	13749
D-24-05	halite	24496	12928
D-24-06	gypsum	22786	13072
D-24-07	halite	25445	10523
D-24-08	halite	38907	8344
D-24-09	gypsum	5124	23377
D-24-10	gypsum	1101	28403
D-24-11	gypsum	7683	2878
D-24-12	gypsum	582	19458
D-24-13	lam	5830	1385
D-33-01	halite	40593	8616
D-33-02	gypsum	761	20187
D-33-03	halite	40231	10020
D-33-04	gypsum	4694	38411
D-33-05	lam	7119	1818
D-34-01	halite	93556	1389
D-34-02	gypsum	9412	36339
D-34-03	halite	50594	8128
D-34-04	gypsum	10352	17809
D-34-05	halite	67961	5932
D-34-06	lam	10110	154
D-35-01	halite	78705	3222
D-35-02	gypsum	43256	7650
D-35-03	halite	48120	7020
D-35-04	gypsum	36808	25517
D-35-05	halite	60701	3038
D-35-06	gypsum	15713	12832
D-35-07	halite	52327	7540
D-35-08	gypsum	2938	19500
D-35-09	halite	55617	10535
D-35-10	halite	91761	1474
D-35-11	gypsum	4562	14425
D-35-12	lam	9535	715
D-42-01	halite	72106	1036
D-42-02	gypsum	51731	13544
D-42-03	halite	49775	13224
D-42-04	gypsum	59294	14787
D-42-05	halite	45179	10628
D-42-06	gypsum	16834	19530
D-42-07	gypsum	52548	20929
D-42-08	halite	62986	8073
D-42-09	gypsum	10159	25130
D-42-10	halite	96825	5838
D-42-11	gypsum	16403	21105
D-42-12	halite	101718	2453
D-42-13	gypsum	13936	13768
D-42-14	gypsum	56226	13978

D-42-15	lam	3323	13457
D-42-16	lam	6530	116
D-45-01	halite	101762	1332
D-45-02	gypsum	2505	19983
D-45-03	halite	56369	8972
D-45-04	gypsum	29979	24825
D-45-05	halite	49868	6013
D-45-06	gypsum	4027	22409
D-45-07	halite	43328	10525
D-45-08	gypsum	10848	22175
D-45-09	halite	66453	3980
D-45-10	halite	74109	2768
D-45-11	gypsum	6317	8931
D-45-12	lam	7405	4749
D-45-13	lam	3817	144
D-55-01	halite	85191	4823
D-55-02	gypsum	1774	27446
D-55-03	lam	10781	158
D-60-01	halite	87867	2302
D-60-02	halite	55232	8962
D-60-03	gypsum	3226	24034
D-60-04	halite	51287	7675
D-60-05	gypsum	22685	10944
D-60-06	halite	59104	10211
D-60-07	gypsum	21104	24964
D-60-08	halite	53431	7450
D-60-09	gypsum	1382	23548
D-60-10	gypsum	1997	13815
D-60-11	gypsum	2095	12032
D-60-12	lam	10126	225
D-66-01	halite	77867	1134
D-66-02	gypsum	9328	14095
D-66-03	halite	52797	1835
D-66-04	gypsum	6558	16259
D-66-05	gypsum	311	15487
D-66-06	lam	7188	2296
D-66-07	lam	6220	120
D-08-01	halite	71566	2103
D-08-02	gypsum	14599	15457
D-08-03	halite	28706	14298
D-08-04	gypsum	31396	16080
D-08-05	lam	9026	207

Appendix E. Explanation of GIS methods used in study

In order to compare the 2016 thickness surface with the BLM's modeled surface in 2003, the following inputs and settings identified in White and Terrazas (2006) were used:

- Step 1: Kriging/Cokriging > Ordinary
- Step 2: Transformation Type > None. Order of trend removal > Second.
- Step 3: No change to default values.
- Step 4: Anisotropy > True

Note that all steps in Appendix C correspond with ArcMap's (version 10.4) numbered steps in the Geostatistical Wizard available under the Geostatistical Analyst extension. The kriging analysis was performed in inches as that was the unit of measure used to measure the salt thickness. All other inputs and settings not listed above were assumed to be assigned default values in 2003 and therefore were assigned default values for this study.

White and Terrazas' (2006) thickness interpolation methods were replicated to best compare results and identify any change on BSF. Pre-processing of the thickness surface created with the kriging process described above is needed to calculate volume using ArcMap's 3D Analyst Toolbox extension's Surface Volume tool. Steps are described below:

1. **Clip the output to the BSF boundary:** The tool Extract by Mask (Spatial Analyst Toolbox) was used to limit the file extent to the BSF boundary. The BSF boundary defined by White and Terrazas in 2003 was initially used to provide consistency. The BSF 2003 boundary was digitized from Figure 5's map in White and Terrazas (2006). It should be noted that reported results from White and Terrazas extend beyond the boundary of any interpolated surface, and thus was cropped to the new area shown in Figure 9 for these analyses.
2. **Assign values negative numbers to reflect being below ground:** Raster Calculator (Spatial Analyst Toolbox) was used to assign values in raster to negative with the following expression: - "%RasterName%"
3. **Remove above ground anomalies:** all values at this point in the process that were positive were calculated to 0 using Raster Calculator and the following expression: Con("%RasterName%" > 0 , 0 "%RasterName%"). This ensured that all values were below ground (to represent the depth to clay).
4. **Convert values to meters:** ArcGIS's Surface Volume tool requires that the input units be in meters. To convert from inches to meters, the Times tool was used (Spatial Analyst Toolbox Raster Math Toolset) to multiply all values by 0.0254.
5. **Calculate volume:** The Surface Volume tool (3D Analyst Functional Surface Toolset) was used to calculate volume. The input settings were:
 1. Input surface: raster processed in steps 1-4 above.
 2. Output text file: saved results as a local text file (See Appendix B)
 3. Reference Plane: BELOW
 4. Plane Height: left empty
 5. Z Factor: 1 (default)

To automate the five steps described above, a model was created using ArcGIS's Model Builder.

Various mapping techniques and symbology settings were utilized in ArcMap to create maps to display results of BSF salt thickness data analyses. Two processes are described here for easier replication for future studies.

In order to best display contours (e.g. elevation, thickness), the correct kriging results were exported to vectors. These were the steps taken in this project to produce vector polylines:

1. SA (Spatial Analyst) Contour.
2. Contour Interval: 12.
3. Base Contour: 0.
4. Z Factor: 1.

Note that no other settings were changed unless described above. For analysis requiring a raster file of the kriging results, GA Layer to Grid was used and default settings were retained. To export a GA layer, right mouse click on the layer in ArcMap, and select Export to Raster under Data.

All contours were smoothed in order to improve visual simplicity of spatial patterns for total salt and individual strata thickness. The method used was:

1. (Cartography) Smooth Line.
2. Smoothing Algorithm: PAEK.
3. Smoothing Tolerance: 2000 meters.
4. Check "Preserve endpoint for closed line".
5. Handling Topological Errors: NO_CHECK

Difference values were used at the measurement point scale and a new kriged surface was interpolated (see above for method) to create maps that display the regional and compositional differences across BSF between 2003 and 2016. This method was utilized to map the difference from the results for all salt thickness measurements of total salt thickness depth, salt thickness of the top layer of dense crystallized halite, and total salt thickness of halite and gypsum per each borehole.

Table E-1. Example of 3D analyst volume calculation outputs

	Dataset	Plane Height	Reference	Z_Factor	Area_2D	Area_3D	Volume (m³)
3D Analyst Surface Volume Text output (meters) for 2016 total salt thickness kriging surface	..016_mask_negative_NoPos_meters	0	BELOW	1	93802689	93802696.8	67464024.48
3D Analyst Surface Volume Text output (meters) for 2003 total salt thickness kriging surface	..003_mask_negative_NoPos_meters	0	BELOW	1	93802689	93802697.88	72479238.96

APPENDIX E FIGURE CAPTIONS

Figure E-1. Arc GIS Geostatistical Wizard screen shot examples of steps used in kriging.

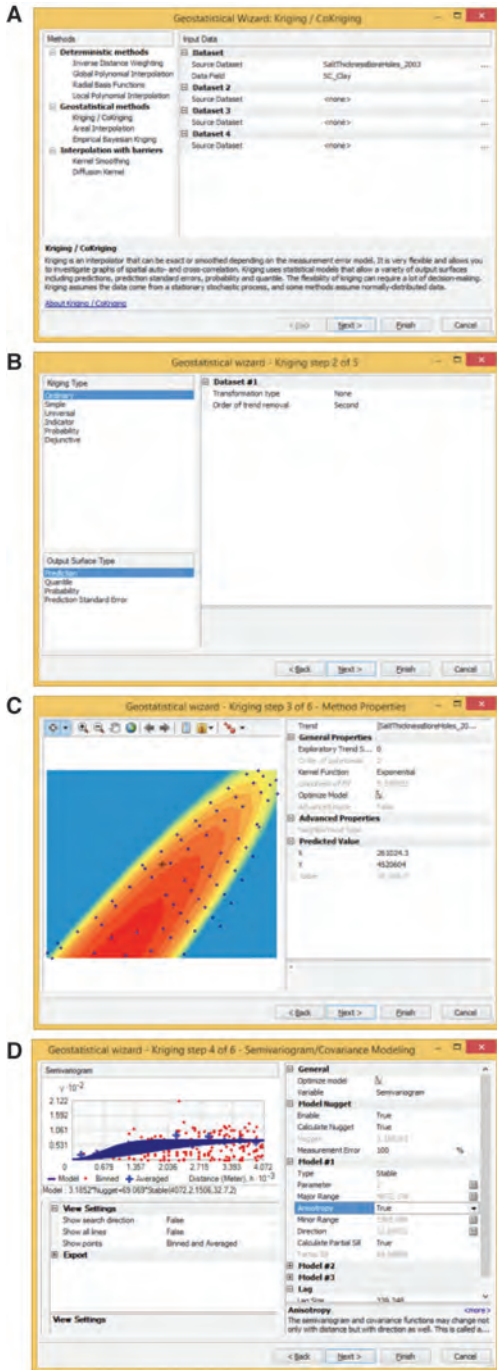
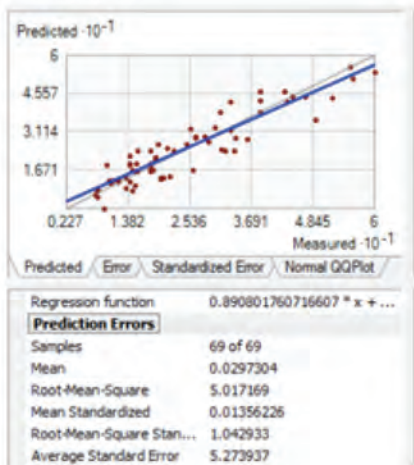


Figure E-2. Arc GIS screen shot examples of data kriging prediction errors (inches) from replication of 2003 kriging (A) and 2006 data (B).

A 2003 data



B 2016 data

